Erosion and mobility in granular collapse over sloping beds

A. Mangeney,[1] O. Roche,[2] O. Hungr,[3] N. Mangold,[4] G. Faccanoni,[1,5] and A. Lucas[1]

Received 23 July 2009; revised 18 March 2010; accepted 30 March 2010; published 25 September 2010.

[1] We describe laboratory experiments of granular material flowing over an inclined plane covered by an erodible bed, designed to mimic erosion processes of natural flows travelling over deposits built up by earlier events. Two controlling parameters are the inclination of the plane and the thickness of the erodible layer. We show that erosion processes can increase the flow mobility (i.e., runout) over slopes with inclination close to the repose angle of the grains θ_r by up to 40%, even for very thin erodible beds. Erosion efficiency is shown to strongly depend on the slope of the topography. Entrainment begins to affect the flow at inclination angles exceeding a critical angle $\theta_c \simeq \theta_r/2$. Runout distance increases almost linearly as a function of the thickness of the erodible bed, suggesting that erosion is mainly supply-dependent. Two regimes are observed during granular collapse: a first spreading phase with high velocity followed by a slow thin flow, provided either the slope or the thickness of the erodible bed is high enough. Surprisingly, erosion affects the flow mostly during the deceleration phase and the slow regime. The avalanche excavates the erodible layer immediately at the flow front. Waves are observed behind the front that help to remove grains from the erodible bed. Steep frontal surges are seen at high inclination angles over both rigid or erodible bed. Finally, simple scaling laws are proposed making it possible to obtain a first estimate of the deposit and emplacement time of a granular collapse over a rigid or erodible inclined bed.

Citation: Mangeney, A., O. Roche, O. Hungr, N. Mangold, G. Faccanoni, and A. Lucas (2010), Erosion and mobility in granular collapse over sloping beds, *J. Geophys. Res.*, *115*, F03040, doi:10.1029/2009JF001462.

1. Introduction

[2] Avalanches and landslides play a significant role in erosion processes at the surface of the Earth and other telluric planets. On Earth, they represent a threat for population and infrastructure in volcanic, mountainous, seismic, or coastal areas. The research field dealing with dynamic analysis of gravitational mass flows is rapidly expanding. One of its ultimate goals is to produce tools for prediction of velocity and runout extent of rapid landslides. Of special interest are experimental, theoretical and modeling developments that can help explain the occurrence of rapid motion over long distances [e.g., *Legros*, 2002; *Lucas and Mangeney*, 2007]. Despite the great amount of work devoted to the study of landslides and avalanches, there is no consensus to explain the high mobility of avalanches or the occurrence of surges (i.e., steep fronts) that can propagate along the slope without decelerating. Some of the most dangerous and mobile landslide types on Earth exhibit surging behavior.

[3] Several mechanisms have been suggested to explain the high mobility of gravitational flows, e.g., upward current of air, hovercraft action at the base, melting of rock, fluidization induced by the presence of fine dust, acoustic fluidization, frictional heat, hydroplanning, or the potential presence of water or air within the granular mass (see *Legros* [2002] and *Pudasaini and Hutter* [2007] for a review). Recent studies also point out the effects on granular flow mobility of the initial fluidization of the material [*Roche et al.*, 2002, 2004, 2008; *Girolami et al.*, 2008], of the polydispersity and shape of the particles [*Goujon et al.*, 2007], and of the fragmentation of grains [*Davies et al.*, 1999].

[4] Our goal in this paper is to show that erosion of granular material already present on the bed can significantly increase the mobility of avalanches flowing on moderate slopes under certain circumstances. Furthermore, when the slope lies between the repose angle θ_r and avalanche angle θ_a of the material, surging fronts can develop, propagating at almost constant velocity.

[5] As rock avalanches, debris and pyroclastic flows hurtle down mountain and valley slopes on Earth and on Mars, they often entrain bed material along their way [e.g., *Suwa and Okuda*, 1980; *Hungr et al.*, 1984; *Benda*, 1990; *Sparks et al.*, 1997; *Berti et al.*, 2000; *Calder et al.*, 2000; *Wang et al.*, 2003; *Papa et al.*, 2004; *Stock et al.*, 2005; *Stock and Dietrich*, 2006; *Bonnard et al.*, 2009; *Mangold et al.*,

[1]Institut de Physique du Globe de Paris, Equipe Sismologie, CNRS-UMR 7154, Université Paris Diderot 7, Paris, France.
[2]Clermont Université, Université Blaise Pascal, Laboratoire Magma et Volcans, CNRS-UMR 6524, IRD-R163, France.
[3]University of British Columbia, Vancouver, British Columbia, Canada.
[4]Laboratoire de Planétologie et Géodynamique de Nantes, Université de Nantes, CNRS-UMR 6112, France.
[5]IMATH, Université du Sud, Toulon-Var, France.

0148-0227/10/2009JF001462

2010]. Field studies even suggest that bedrock incision by natural granular flows may be the primary process cutting valleys in steep, unglaciated landscapes (see references in the work of *Hsu et al.* [2008]). Erosion and entrainment of bed material can play a significant role in the mobility of landslides and debris or snow avalanches and overall dynamics of transportation [e.g., *Sovilla and Bartelt*, 2002; *Hungr and Evans*, 2004; *McDougall and Hungr*, 2004; *Sovilla et al.*, 2006; *Crosta et al.*, 2009a, 2009b]. Entrainment of the substrate by a flowing mass could either accelerate or decelerate the flow (i.e., increase or decrease its mobility) depending on the nature of the erodible material as well as on the topography and on the dynamics of the flow.

[6] Quantitative aspects of erosion processes have, however, so far been insufficiently studied in the field and in the laboratory as well as in numerical models. As a first attempt to address this issue, we devised laboratory experiments using the simplest case of dry granular material flowing over an inclined plane covered by a thin erodible bed made of the same material. The goal is to mimic the geometry of natural debris flows or avalanches flowing on deposits built up by earlier events.

[7] Most experiments dealing with dry granular flows over a planar substrate have been conducted on moderately steep slopes at angles $\theta \in [\theta_r, \theta_a]$ [*Groupement De Recherche Milieux Divises* (*GDR MiDi*), 2004; *Pudasaini and Hutter*, 2007] or on horizontal beds ($\theta = 0$) [e.g., *Lube et al.*, 2004; *Lajeunesse et al.*, 2004; *Siavoshi and Kudrolli*, 2005; *Balmforth and Kerswell*, 2005] (see also references in the work of *Bouchut et al.* [2008] and *Lacaze et al.* [2008]). For a granular collapse over a horizontal plane, the dynamics is controlled by the balance between pressure gradient, inertia, and friction. On the contrary, flows over moderately inclined plane depend essentially on the balance between gravity and friction. Surprisingly, only a few recent studies focus on the influence of the inclination angle on the flow dynamics [*Hogg*, 2008; *Hungr*, 2008].

[8] Several experimental studies have been done on granular flows over thin or thick layers of erodible material in the so-called metastable domain ($\theta \in [\theta_r, \theta_a]$). In this range of inclination *Pouliquen and Forterre* [2002] show that when a three-dimensional granular cap is released on an inclined bed covered by a shallow erodible bed built up of the same granular material, triangular shaped traveling waves are created propagating at constant velocities down-slope. Triangular shaped quasi-one-dimensional waves have also been observed and studied theoretically when a perturbation is imposed at the top of a thin granular layer over an inclined plane [*Mallogi et al.*, 2006; *Aranson et al.*, 2006] or when a constant flux of material is imposed on top of the plane [*Börzsönyi et al.*, 2005, 2008]. Using the partial fluidization model proposed by *Aranson and Tsimring* [2002] and *Aranson et al.* [2008], *Mangeney et al.* [2007a] show that the presence of even a very thin layer of granular material lying on the solid bed strongly increases the mobility of granular flows when the inclination of the erodible bed is near the metastable domain. Furthermore, as the thickness of the granular layer increases, the dynamics of the flowing mass dramatically changes from a decelerating avalanche to a traveling wave.

[9] Experimental and numerical results thus show that erosion processes significantly increase the mobility of a granular mass flowing over an erodible bed, in the inclination range $\theta \in [\theta_r, \theta_a]$. The question is whether similar effects occur on gentler slopes, i.e., outside the metastable domain $\theta < \theta_r$. Significant difference in the effect of erosion processes on avalanche flows is expected depending on the inclination angle of the erodible bed, compared to the friction angles of the involved material. To our knowledge, no studies have been done to explore this issue. The questions we want to address are as follows:

[10] 1. Does the presence of an erodible bed always accelerate avalanche flow that travel over an inclined plane?

[11] 2. How does the mobility (i.e., the runout distance) change when the thickness of the erodible bed increases?

[12] 3. How do these effects depend on the slope of the topography?

[13] 4. Is there a critical slope and/or thickness of the erodible bed, for a given granular material, separating different regimes of erosive avalanches (deceleration, acceleration, surge formation…)?

[14] In section 2, we first show evidence of erosion processes on Earth. After describing the experimental setup in section 3 and providing basic theoretical concepts and scaling laws in section 4, we present in section 5 experimental results of granular collapse over a rough rigid plane with inclination varying from horizontal to moderate slope. The influence of a thin erodible layer covering the plane on the flow dynamics and on the deposit is then investigated in section 6. In section 7, observations are provided on the internal motion within the flowing and erodible layers and on waves that propagate within the granular flow. In section 8, these results are discussed to shed light into erosion effects on avalanche behavior as an attempt to help further validate numerical models of avalanches and associated erosion/depositon laws and to improve assessment of avalanche mobility.

2. Field Evidence of Erosion Processes

[15] Field evidence of bed material entrainment has been observed in various environments on Earth, involving snow and debris avalanches, debris flows, or pyroclastic flows. Even though erosion processes are very different depending on the nature and volume of the flowing and erodible material involved as well as on the initial and boundary conditions, examples of qualitative observations, focusing on dense flows, are gathered here to highlight some characteristics of natural erosion processes (penetration depth, nature, localization and volume of eroded material, topography …).

[16] Material entrainment under natural conditions occurs more often on steep slopes, although entrainment on flatter slopes may occur as well. The entrainment process is often observed to be supply-limited, so that the amount of material involved is limited to the depth of a weak erodible layer [*Hungr et al.*, 2005; *Sparks et al.*, 1997].

[17] Often, erodible material on slopes consists of deposits of former events. Accumulations of such deposits form a colluvial apron (Figures 1 and 2). Natural flows may form deposits at very different angles depending on the flow regime. As an example, pyroclastic flows may generate deposits on slopes near to the repose angle of the material involved [*Felix and Thomas*, 2004; *Mangeney et al.*, 2007b]. On the other hand some highly energetic pyroclastic flows and landslides form deposits on slopes much smaller than the

Figure 1. Deposit of pyroclastic flows occurring during the 2003 eruption on the slope of the Lascar volcano, Chile. The deposits can be observed on slopes varying from 4° to 14°. A field survey described by Jessop et al. (manuscript in preparation, 2010) shows that most of the pyroclastic flows were flowing on deposits of former events. Picture Anne Mangeney, 2007.

friction angle characterizing the flowing material. This is due to other driving forces than gravity (inertia, pressure gradient) that make it possible for the material to flow even though the gravity force along the slope is smaller than the frictional dissipation [see, e.g., *Mangeney-Castelnau et al.*, 2003, Figures 13 and 16].

[18] The volume of a flowing avalanche can be dramatically increased through entrainment of bed material as shown in Figure 2a representing a segment of fine-grained colluvial soil eroded by the passage of a rock avalanche. The rock debris in this case had a volume of over 3×10^5 m^3, while the erosion scar yielded nearly the same volume, as shown by a ground survey. Entrainment zones have been observed on slopes ranging from 25° to 35°. Similar evidence of entrainment has been described in many case histories. A small selection from cases reviewed by *Hungr and Evans* [2004] and *Hungr et al.* [2005] is given in Table 1 for illustration.

[19] Wet debris flows are frequent in alpine and artic environments and can occur at slopes as low as 10°. As these debris flows occur mainly on cohesionless fans and debris aprons, entrainment of boulders by the flow is frequent, and erosion takes place at the base of the channel. The example of Figure 2b shows a debris flow near the Izoard pass (southern French Alps). This flow formed in the summer 1995 from a heavy rainfall that created several debris flows in this region [*Lahousse and Salvador*, 1995]. The upper section of the observed channel is purely erosional (no levees, >5 m incision over a 25°–30° steep slope) with a progressive transition into a channelized flow (3 m high levees over a 15° steep slope). At the location of levees, the flow was still erosive: the 15 m wide channel is about 1 m deeper than the base of the debris aprons, as shown from the difference in levees thickness inside and outside the channel (Figure 2b). Note that, at the surface of the planet Mars, gullies formed on steep slopes indicate similar erosion inside debris aprons [*Malin and Edgett*, 2001; *Mangold et al.*, 2003; *Mangold et al.*, 2010].

[20] On Lascar volcano, Chile, pyroclastic flows generated by the 1993 eruption produced spectacular erosion features where flows accelerated through topographic restrictions or where they moved over steep slopes [*Sparks et al.*, 1997; *Calder et al.*, 2000] (Figure 1). Erosion furrows 0.1–0.3 m deep formed as a result of flows with maximum thickness of a few meters. Short striae at different angles, impact marks,

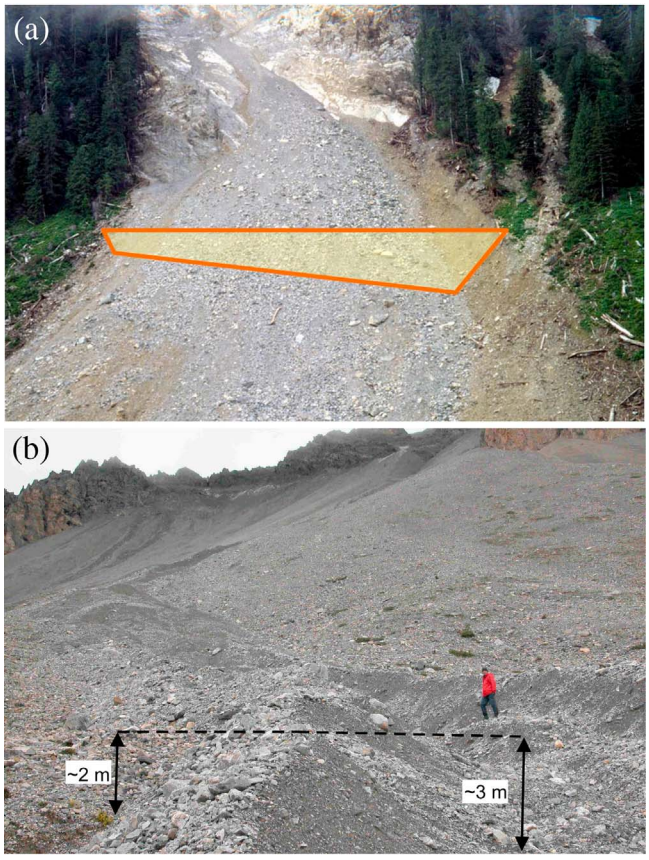

Figure 2. (a) Erosion scar excavated in a colluvial apron by a 3×10^5 m^3 rock avalanche. The mean depth of the eroded zone, as indicated by a schematic cross section, is approximately 8 m. The base of the scar is partly filled by rock debris. The scar is approximately 100 m wide (Nomash River rock slide debris avalanche, Vancouver Island, British Columbia, Canada, 1999. After *Hungr and Evans* [2004]). (b) Debris flows at Izoard Pass (French Alps), closeup on a leveed channel. The external part of the channel is shallower than the internal part showing a net erosion of about 1 m.

Table 1. Selected Examples of Rock and Debris Avalanches Involving Significant Entrainment[a]

Case	Initial Slide Volume (m^3)	Entrained Volume (m^3)	Slope Angle of the Entrainment Zone	Entrained Material
Huascaran, Peru, 1970 rock and ice avalanche	13×10^6	39×10^6	20°–45°	Glacial till and ice
Mt. Ontake, Japan, 1984 volcanic rock avalanche	34×10^6	22×10^6	20°–45°	Colluvium and alluvium
Nomash River, Canada, 1999 rock slide-debris avalanche	3×10^5	3×10^5	25°–35°	Till-derived colluvium
Tsing Shan, Hong Kong, 1990 debris flow	400	19 600	23°–35°	Colluvium, residual soil

[a]Based on *Hungr and Evans* [2004] and *Hungr et al.* [2005].

and mixing of bedrock-derived lithic clasts throughout the deposits indicate that internal mixing was allowed to occur within the flow [*Sparks et al.*, 1997].

[21] Entrainment increases runout in some situations but decreases in others. As shown by field measurements, snow avalanches may entrain significant amounts of snow and increase their runout distance compared to non erosive avalanches occurring on the same topography [*Sovilla et al.*, 2001, 2006]. On the other hand, during the 2007 avalanche period in the Austrian Alps, many snow avalanches were stopped because they had to entrain heavy, wet snow covers in the runout zone. In that case, entrainment decreased dramatically the mobility of the flows. Depending on the nature and volume of the snow, very different potential mechanisms of entrainment have been reported in the literature [*Gauer and Issler,* 2003; *Ancey*, 2004].

[22] Long runout distances are observed for debris flows forming steep, bulbous flow fronts, hereafter called surges, that are known to travel on relatively flat angles at nearly constant velocities [e.g., *Pierson*, 1980; *Takahashi*, 1991; *Hungr et al.*, 2001]. Processes leading to the formation of surges have been studied by many, both in the field and theoretically [e.g., *Takahashi*, 1991; *Savage and Iverson*, 2003; *Zanuttigh and Lamberti*, 2007]. However, no well-established theoretical model exists at present. The observation made in this paper is that dry granular flows over rigid and erodible beds can, in fact, develop surging fronts that can travel at almost constant velocities, if they occur at inclinations very close to the friction angle of the material.

[23] In the very simplified framework of our granular flow experiments, we will investigate quantitatively the effect of slope and of erodible material availability on erosion processes, the penetration depth into the erodible bed, the mixing of erodible and flowing grains, and the potential occurrence of surges propagating along the slope.

3. Experimental Setup

[24] The experimental setup consists of a narrow channel between Plexiglas walls, spaced by 10 cm. The planar channel is 3 m long with possible inclinations varying from horizontal up to 30° (Figure 3). A rectangular granular mass of thickness $h_0 = 14 \pm 0.5$ cm (around 215 particle diameters) and of down-slope length $r_0 = 20 \pm 0.5$ cm (around 286 particles), i.e. an aspect ratio $a = h_0/r_0 = 0.7$, is released from a reservoir at time $t = 0$ s, as shown in Figures 4 and 3. The granular material flows down an inclined channel covered by an erodible bed of variable thickness at different inclination angles.

[25] We used glass beads of diameter $d \in [600, 800]$ μm that were subspherical, cohesionless, and highly rigid. Though the characteristics of these particles may be similar to those of some natural rock avalanches, they may differ substantially from those of most snow avalanches. In the latter case, aggregation of the snow particles or, in contrast, attrition generated by collisions, are likely to change the properties of the particles during propagation. The repose angle $\theta_r = 23.5° \pm 0.5°$ and the avalanche angle $\theta_a = 25.5° \pm 0.5°$ of the material have been measured by adding material on top of a pile at a small rate and measuring the angle of the pile with the horizontal after and before an avalanche, respectively. The

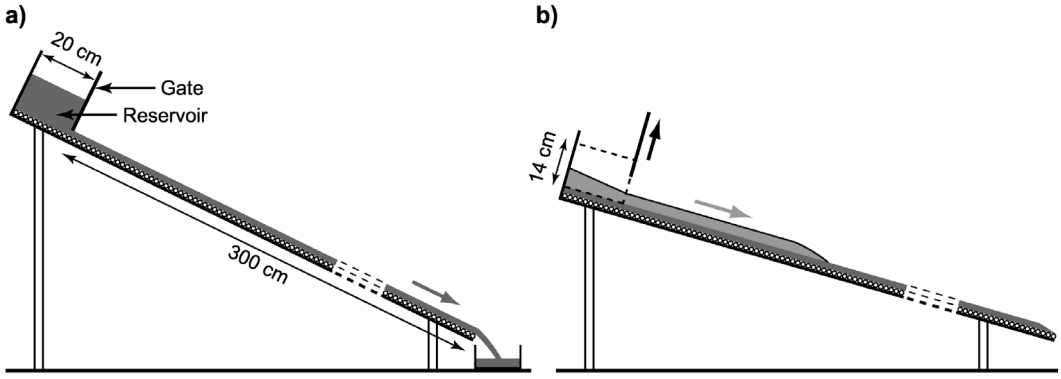

Figure 3. Experimental setup: schematic representation of (a) the 2-D channel and the reservoir inclined at $\theta \in [\theta_1, \theta_2]$ with $\theta_1 \simeq \theta_r$ and $\theta_2 \simeq \theta_r + 8°$, where the erodible bed (colored in dark gray) is built up by closing the gate once steady uniform flows are created, (b) the flow (colored in light gray) on top of the erodible bed over a sloping channel inclined at $\theta \leq \theta_r$ created by opening the gate at the initial instant.

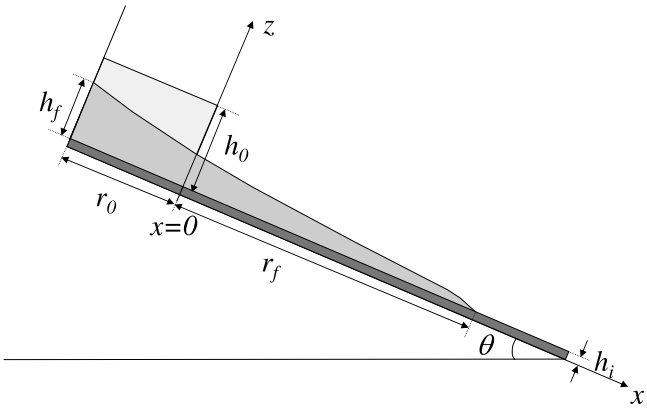

Figure 4. Morphometric and control parameters measured in the experiments. The initial mass (light gray) with initial thickness h_0 = 14 cm and radius r_0 = 20 cm (aspect ratio a = 0.7) is released on a plan with inclination θ covered by an erodible bed of thickness h_i (dark gray). It forms a deposit (moderate gray) with a length r_f from r_0, hereafter called the runout distance, and a final maximum thickness h_f.

density ρ = 2500 kg m^{-3} and porosity ν = 0.62 of the beads were estimated.

[26] Basal roughness was provided by gluing a single layer of the same particles to the channel base. The uniform thin layer of erodible bed was formed by steady uniform flows travel down the inclined plane and suddenly cutting the supply to allow the layer to deposit (see section 4 and Figure 3a). Once the deposit of thickness h_s is obtained, the slope is slowly lowered to the angle required for the experiments (Figure 3b). Alternatively, erodible beds could have been built up by levelling their top with a plate within the channel in the horizontal position, and then subsequently inclined to run the experiments, but this might have led to various degrees of compaction of the material along the channel, which we wanted to avoid as much as possible.

[27] Experiments have been performed first on a rough rigid bed at inclination angles $\theta = 0°$, $\theta = 10°$, $\theta = 16°$, $\theta = 19°$, $\theta = 22°$, $\theta = 23.7°$, and $\theta = 25.2°$ (section 5) and then on the same plane but covered by a thin erodible layer of variable thickness $h_i \in [1,6]$ mm, i.e., $h_i/d \in [1,8]$ (section 6). As a result, the two control parameters of the system are the inclination angle of the plane θ and the thickness of the erodible bed h_i. The angles have been measured with a precision $\delta\theta = 0.3°$ and the thickness of the erodible bed h_i with a precision varying from δh_i = 0.1 mm to δh_i = 1 mm for h_i varying from 1 to 6 mm due to slight variation of h_i along the slope. Table 2 summarizes the characteristics of the experiments.

[28] The length of the deposit r_f measured from the front of the initial mass located at x = 0, i.e., the runout distance, and the final thickness of the deposit at the upper wall h_f (Figure 4) have been systematically recorded as well as the time at which the front stops t_f. The profiles of the granular mass as a function of time have been measured using a high-speed camera.

[29] The internal velocity in the body of the flow has been measured along the transparent sidewall of the channel. We used colored (black) particles of the same size and character as that in the flow as tracers, and these were added to the granular mass in proportions up to 10 vol % to allow visualization of their motion from high-speed videos at 150–200 frames/s. Measurements were made from successive frames during short time intervals of 0.01–0.04 s. It has been checked that the presence of these particles does not change the dynamics of the flow. Results showed that paths of neighboring particles were almost linear and parallel to each other and to the channel substrate. We acknowledge that the velocity profiles thus determined might have been influenced by sidewall effects. However, complementary measurements made at the surface of the flows revealed that the velocity profiles perpendicular to the channel walls were linear, though slightly curved near the margins. This showed that the resistance imposed by the walls was very small and that the velocity profiles measured at the sides was representative of those in the flow interior. Some experiments have been replicated using colored black particles for the erodible layer in order to visualize the potential mixing of flowing and initially static material (experiments E′ in Table 2). Black particles had a slightly higher repose angle than the regular beads, possibly due to mild cohesion effects ($\theta_{rb} \sim 28° > \theta_r$).

4. Theoretical Framework

[30] Before presenting the experimental results, let us recall observations and theoretical tools that make it possible to describe the basic behavior of dry granular flows, that were used here both to build up the erodible layers and to interpret the results.

Table 2. Characteristics of the Different Experiments[a]

Experiment	Angle θ (°)	Thickness h_i (mm)	Runout (cm)
E0-0	0	0	27.5 ± 1.5
E0-1.4	0	1.4	25 ± 0.2
E0-3.2	0	3.2	24.9 ± 0.6
E0-6.5	0	6.5	25.1 ± 0.9
E10-0	10 ± 0.2	0	43.5 ± 2.5
E10-1.03	10 ± 0.2	1.03	41.25 ± 0.75
E10-1.7	10 ± 0.2	1.7	43 ± 1
E10-3.14	10 ± 0.2	3.14	42.5 ± 1.5
E10-4.76	10 ± 0.2	4.76	42 ± 1
E16-0	16 ± 0.1	0	62 ± 1.6
E16-1.4	16 ± 0.1	1.4	63 ± 2.5
E16-2.5	16 ± 0.1	2.5	67 ± 2
E16-5	16 ± 0.1	5	68 ± 2.5
E19-0	19 ± 0.1	0	87 ± 3
E19-1.5	19 ± 0.1	1.5	89 ± 2
E19-2.7	19 ± 0.1	2.7	96 ± 2.3
E19-5.3	19 ± 0.1	5.3	102 ± 3.5
E22-0	22 ± 0.1	0	108 ± 3.2
E22-1.82	22 ± 0.1	1.82	119.25 ± 3.25
E′22-3	22 ± 0.1	3.01	Not measured
E22-3.38	22 ± 0.1	3.38	131.5 ± 3.5
E22-4.6	22 ± 0.1	4.6	151 ± 3
E′22-5	22 ± 0.1	5	Not measured
E24-0	23.7 ± 0.1	0	179 ± 3.2
E24-1.82	23.7 ± 0.1	1.4	out of plane
E25-0	25.2 ± 0.2	0	out of plane
E25-2	25.2 ± 0.2	2	out of plane
E25-3.6	25.2 ± 0.2	3.6	out of plane
E′25-3.9	25.2 ± 0.2	3.9	out of plane
E′25-5	25.4 ± 0.2	5	out of plane

[a]Experiments E′ are designed for measurements of internal motion within the flowing and erodible layer and consist of releasing regular glass beads over a layer of erodible bed made of the same beads colored in black (see section 7).

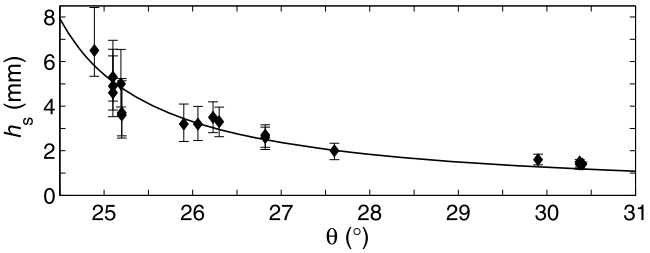

Figure 5. Thickness h_s left on a plane of inclination angle θ after steady uniform flows once the supply is cut. The full line is the best fit to the formula (1) $h_s = \alpha d/(\tan\theta - \tan\delta_1)$ with $\alpha = 0.26$ and $\delta_1 = 23.4°$.

[31] As stated in section 3, the granular erodible bed has been created by the deposit of steady uniform flows in the inclined channel. Indeed, thin, steady uniform granular flows can be observed within a range of inclination angles [e.g., *Savage*, 1979; *Pouliquen*, 1999]. When the supply is cut, these flows leave a uniform deposit along the plane with a thickness $h_s(\theta)$. In our experiments, steady uniform flows occurred for $\theta \in [24°, 32°]$. The curve $h_s(\theta)$ obtained here is shown in Figure 5. Here h_s represents the minimum thickness for flow at a given angle θ [*Pouliquen*, 1999]. A good fit of the experiments is found using the expression proposed by *Börzsönyi et al.* [2008]

$$h_s(\theta) = \frac{\alpha d}{\tan\theta - \tan\delta_1} \tag{1}$$

with $\alpha = 0.26$ and $\delta_1 = 23.4°$. Note that the value of the fitted parameter α is the same as that found by *Börzsönyi et al.* [2008] for glass beads and that the angle δ_1 is very close to the repose angle of the material (also in agreement with *Börzsönyi et al.* [2008]). The formula proposed by *Pouliquen and Forterre* [2002] for $h_s(\theta)$ gives a poorer fit to the results. This method makes it possible to build up erodible beds with thicknesses $h_i \in [1,6]$ mm (see Figure 5). Note that this method only applies for $\theta \in [24°, 32°]$. For $\theta < 24°$, the flow stops very rapidly near the supply and for $\theta > 32°$, the flow does not leave any deposit on the rigid bed.

[32] Analytical solution as well as experimental results show that the deviation of the inclination angle of the plane θ from the friction angle of the material involved δ (close to the repose and avalanche angles)

$$\tan\theta - \tan\delta, \tag{2}$$

is a key parameter in the description of granular flows, in agreement with equation (1) [*Mangeney et al.*, 2000; *Mangeney-Castelnau et al.*, 2005; *Kerswell*, 2005; *Hogg*, 2008; *Börzsönyi et al.*, 2008; *Fischer et al.*, 2008]. Even though the analytical solution of *Mangeney et al.* [2000] has been derived for the release of a dam with infinite dimension in the upslope direction, simple scaling laws can be deduced from this solution that can help define empirical relations for describing the granular flows investigated here. Note that analytical solutions for the release of a finite initial mass with various geometries have been recently developed [*Kerswell*, 2005; *Fernandez-Feria*, 2006; *Ancey et al.*, 2008]. From the analytical solution of *Mangeney et al.* [2000] the front position can be calculated as

$$x_f = 2c_0 t + \frac{1}{2} m t^2. \tag{3}$$

where $c_0 = \sqrt{k g h_0 \cos\theta}$ and $m = g\cos\theta\,(\tan\theta - \tan\delta)$ is the constant x-acceleration resulting from the sum of the forces due to gravity and friction. The coefficient k is equal to 1 when isotropy of normal stress is imposed or $k = k(\delta, \phi)$ when using the Mohr-Coulomb theory introduced by *Savage and Hutter* [1989], δ and ϕ being the basal and internal friction angles, respectively. The selection of the actual value for k is discussed in section 5. The front stops when $v_f = 2c_0 + m t_f = 0$, so that the stopping time is

$$\frac{t_f}{\tau_c} = \frac{2\sqrt{k}}{\tan\delta - \tan\theta}. \tag{4}$$

where $\tau_c = \sqrt{h_0/(g\cos\theta)}$. Interestingly enough, this relation shows that the time duration of an avalanche is inversely correlated with the deviation of the inclination angle of the bed from the friction angle of the material, being smaller for large deviation. Finally, the runout distance (i.e., final position of the front) $r_f = x_f(t_f)$ is

$$\frac{r_f}{h_0} = \frac{2k}{\tan\delta - \tan\theta}. \tag{5}$$

Note that even though the analytical solution developed by *Mangeney et al.* [2000] was derived for $\theta > \delta$ and for an infinite volume of material in the upslope direction, it leads to the same relations (4) and (5) as the analytical solution proposed by *Kerswell* [2005] for $\theta < \delta$ and for a finite released mass. This is related to the fact that whatever the initial conditions for the released mass or the friction and inclination angles, the perturbation due to the upslope boundary condition never catches up with the front of the flow as demonstrated by *Kerswell* [2005] and *Hogg* [2008]. On the contrary, the final thickness at the upslope wall h_f is obviously affected by the upslope boundary conditions and the expression derived for an infinitely long reservoir (dam) does not correspond to the solution obtained by *Kerswell* [2005]. To further fit the maximum thickness h_f measured experimentally, we use here the semianalytical solution developed by *Kerswell* [2005] and the asymptotic analysis performed by *Hogg* [2008]

$$\frac{h_f}{h_0} = \beta\left(\frac{\tan\delta - \tan\theta}{ak}\right)^{\frac{2}{3}}, \tag{6}$$

where β will be considered here as an empirical parameter. Note that the simple scaling laws (4) and (5) make it possible to recover the relations obtained by *Fischer et al.* [2008] for granular avalanches in a rotating drum.

[33] As shown by *Mangeney-Castelnau et al.* [2005], *Kerswell* [2005] and *Hogg* [2008], the fit of experimental results using analytical or numerical models based on the thin layer approximation such as equations (4) and (5) requires the use of empirical friction coefficients higher than those measured experimentally. The potential reasons for this are discussed in *Mangeney-Castelnau et al.* [2005], *Mangeney et al.* [2006], and *Hogg* [2008]. Here, equations (4), (5),

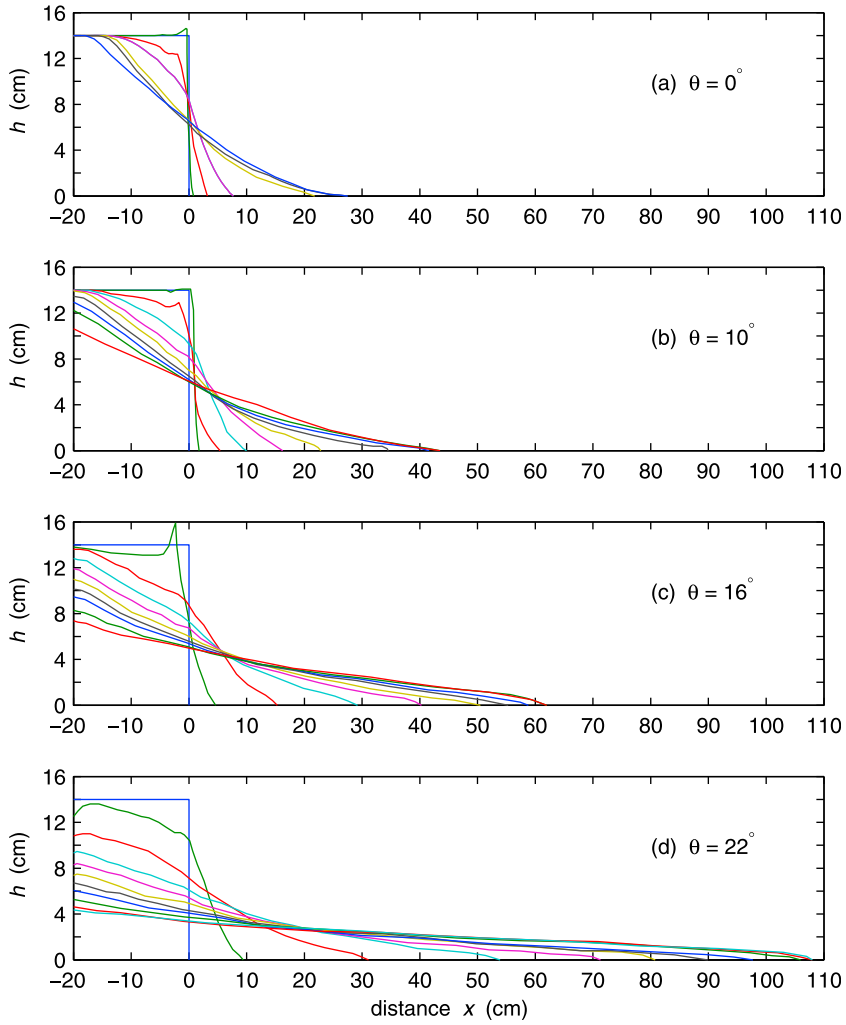

Figure 6. Thickness profile of the granular mass as a function of the downslope position along the plane for the flow over a rigid bed with inclination angle (a) $\theta = 0°$ at time $t = 0$ s, 0.06 s, 0.12 s, 0.18 s, 0.24 s, 0.36 s, 0.5 s, 1.06 s; (b) $\theta = 10°$ at time $t = 0$ s, 0.06 s, 0.12 s, 0.18 s, 0.24 s, 0.3 s, 0.42 s, 0.54 s, 0.68 s, 1.32 s; (c) $\theta = 16°$ at time $t = 0$ s, 0.12 s, 0.24 s, 0.36 s, 0.48 s, 0.6 s, 0.72 s, 0.84 s, 0.96 s, 1.12 s, 1.36 s, 1.62 s; and (d) $\theta = 22°$ at time $t = 0$ s, 0.16 s, 0.32 s, 0.48 s, 0.64 s, 0.8 s, 0.96 s, 1.12 s, 1.44 s, 1.76 s, 2.3 s. These experiments are referred to as E*i*-0, $i = 0$, 10, 16, 22 in Table 2.

and (6) are simply taken as empirical relations with three empirical parameters δ, k, and β that will be fitted to the experimental results. Note that for flows over inclined plane, the downslope acceleration significantly extends the runout relative to flows over horizontal surfaces and much of the flow occurs in thin layers. Therefore thin layer analytical solutions are more likely to represent the dynamics accurately.

[34] Finally, a new analytical solution is developed in Appendix A to interpret the results of granular flows over a thin erodible bed. The analytical solution of *Stoker* [1957] for the horizontal dam break problem of an inviscid (frictionless) fluid on a "wet" bed is extended to the dam break of a frictional material over inclined plane covered by a thin layer made of the same frictional material.

5. Collapse Over Inclined Rigid Bed

[35] Let us first look at the effect of slope inclination on the dynamics and deposit of the granular mass over a rigid bed. Deposits on the plane are obtained only for inclination angles $\theta \leq 23.7° \simeq \theta_r$. For higher inclination angles, the front leaves the experimental flume. Figure 6 shows the thickness profile as a function of the downslope position at different times during the collapse for inclination angles varying from $\theta = 0°$ to $\theta = 22°$. Obviously, as the angle increases, the deposit extends further down the plane and becomes flatter. The normalized runout distance r_f/h_0, final thickness h_f/h_0 and the time when the front stops t_f/τ_c all show a strong variation when the slope approaches the repose angle of the material θ_r (Figure 7).

[36] The runout distance r_f and the time when the flow stops t_f could be successfully fitted using the formula (5) and (4), respectively (Figure 7). Let us first simply use equations (4) and (5) with $k = 0.4$ and $\delta = 32°$ corresponding to the coefficients used by *Mangeney-Castelnau et al.* [2005] to fit granular collapse of glass beads over horizontal plane (dash-dotted lines in Figures 7a and 7c). The runout distance and the stopping time are well reproduced when using these coeffi-

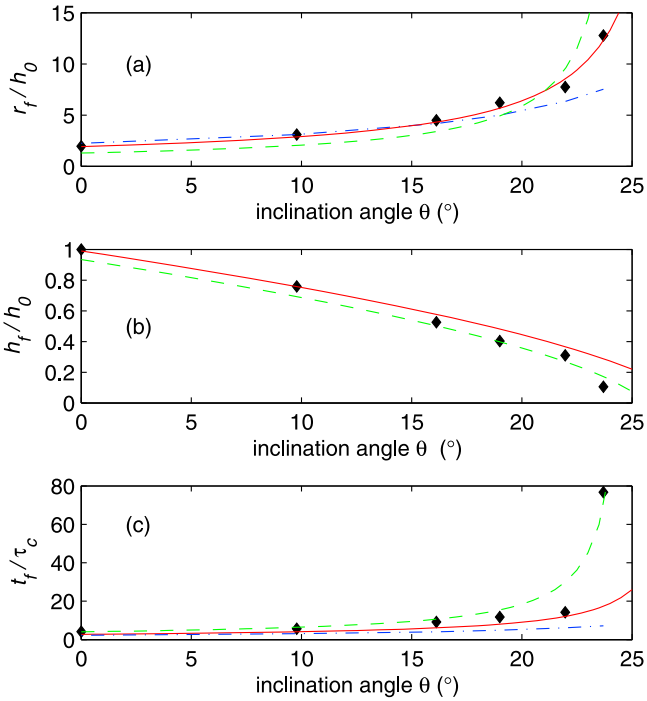

Figure 7. Normalized (a) runout distance r_f/h_0, (b) final thickness at the upper wall h_f/h_0, and (c) time at which the front stops t_f/τ_c where $\tau_c = \sqrt{h_0/(g\cos\theta)}$, as a function of the inclination of the bed θ ($h_0 = 0.14$ m and $\tau_c \in [0.119\text{ s}, 0.124\text{ s}]$ depending on θ). The dash-dotted line corresponds to the analytical fit obtained for granular collapse over horizontal bed ($k = 0.4$ and $\delta = 32°$) by *Mangeney-Castelnau et al.* [2005]; the full line and dashed line are the best fit of the analytical formula (5), (6), and (4) with $k = 0.5$ and friction angles $\delta = 27.5°$ and $\delta = 25.5°$, respectively.

cients for collapse at inclination angles $\theta \leq 15°$. However, when θ gets closer to the friction angle of the material, the experimental runout and stopping time increase more rapidly than the empirical functions. In order to better fit the data, we have calculated the value of the empirical friction angle δ and of the coefficient k that best fit the data. The best fit, obtained with $k = 0.5$ and $\delta = 27.5°$, makes it possible to describe very accurately the change of the runout as a function of the slope inclination and improve the fit of the stopping time for $\theta \leq 22°$. By keeping the value of k and δ, the best fit of the experimental final thickness h_f using equation (6) is obtained for $\beta = 0.76$. However, using these coefficients, the observed change of t_f and h_f when approaching inclination angles $\theta = 23.7°$ is still stronger than that predicted by the empirical relations. This sharp change can only be reproduced by using a friction angle $\delta \simeq 25.5°$ which is indeed closer to the repose and avalanche angles of the material involved (dashed lines in Figure 7).

[37] The mean slope of the deposit with respect to the plane inclination calculated by

$$\theta_f = \arctan\left(\frac{h_f}{r_f}\right) \tag{7}$$

is decreasing almost linearly as a function of the inclination angle (Figure 8). The mean angle of the slope deposit with

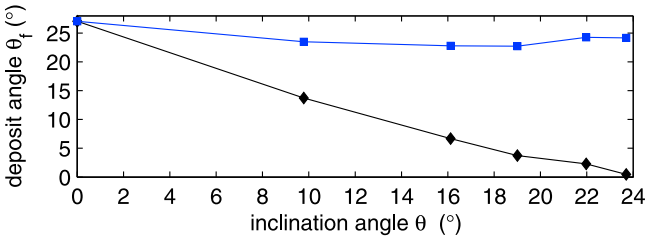

Figure 8. Mean angle of the deposit calculated using equation (7) with respect to the inclined plane (diamond) and with respect to the horizontal direction (squares) as a function of the plane inclination θ.

respect to the horizontal is almost constant and roughly equal to the repose angle of the material $\theta_f + \theta \simeq 24°$.

[38] The position of the front as a function of time $x_f(t)$ is similar to the experimental results of *Hungr* [2008] (Figure 9a). After a transient acceleration at the beginning, the front is observed to move at a nearly constant velocity followed by a transient deceleration before the front stops. The duration of the deceleration phase increases when θ increases (Figure 9a). For $\theta = 23.7°$ a second phase of almost constant velocity

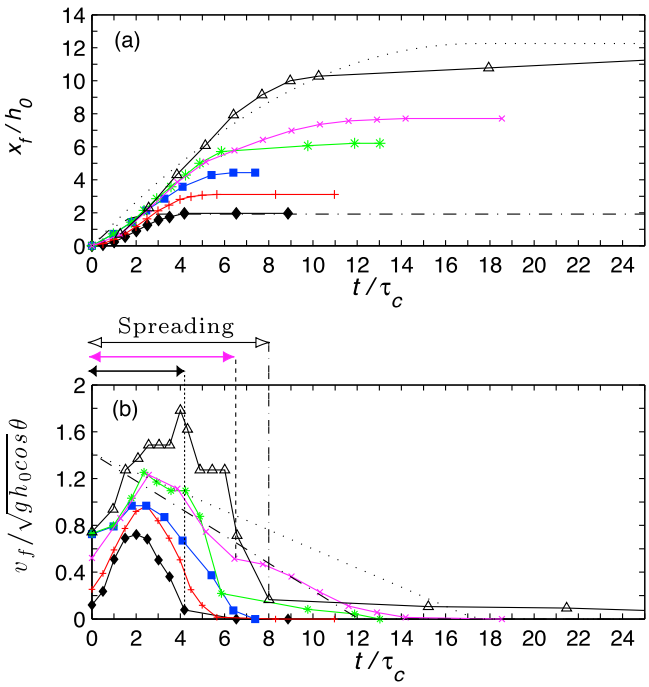

Figure 9. Normalized (a) location of the front $x_f(t)/h_0$ and (b) velocity of the front $v_f(t)/\sqrt{gh_0\cos\theta}$, with $h_0 = 0.14$ m as a function of time t/τ_c, where $\tau_c = \sqrt{h_0/(g\cos\theta)}$ for inclination angle $\theta = 0°$ (diamond), $\theta = 10°$ (cross), $\theta = 16°$ (square), $\theta = 19°$ (star), $\theta = 22°$ (times symbol), and $\theta = 23.7°$ (triangle). The analytical solution (Figure 9a) for the front position (3) at inclination angle $\theta = 0°$ (dash-dotted lines) and $\theta = 23.7°$ (dotted lines) and for the front velocity (Figure 9b) ($v_f(t) = 2c_0 + mt_f$) at inclination angle $\theta = 23.7°$ (dotted) and $\theta = 22°$ (dash-dotted lines) are added. In Figure 9b, the upper arrows represent, from top to bottom, the duration of the spreading regime for $\theta = 23.7°$, $\theta = 22°$, and $\theta = 0°$, respectively.

appears, with a smaller values of the velocity (about 5–15% of the maximum velocity) as shown in Figures 9a and 9b. A similar trend is observed for $\theta = 22°$ and $\theta = 19°$.

[39] Two regimes can be defined from Figure 9b: (1) a so-called spreading regime qualitatively similar to the acceleration/deceleration phases observed for granular collapse over horizontal plane [e.g., *Siavoshi and Kudrolli*, 2005; *Mangeney et al.*, 2006], and (2) a slower quasi-uniform thin flow at velocities of only 5 to 15% of the maximum velocity of the spreading phase. Only the first spreading regime is observed for granular collapse at inclination $\theta \leq 16°$. For higher inclination angles, the second regime is at least initiated, with values of the flow thickness and velocities of the order of those observed for thin steady uniform flows over inclined planes [*Mangeney et al.*, 2007b]. The maximum velocity is reached during the spreading phase and increases with increasing inclination angles (Figure 9b). The duration of the spreading regime also increases with increasing inclination angles.

[40] The analytical equation (3) for $x_f(t)$ differs significantly from the experiments especially in the spreading regime (Figure 9a). The front is moving too fast at the beginning even though the final runout is similar for experimental and analytical results as was observed for granular collapse over horizontal bed by *Mangeney-Castelnau et al.* [2005]. As the slope increases, the analytical solution comes closer to the observations (Figure 9a). However, the two phases of spreading and slow flow cannot be reproduced by the analytical solution that predicts a linear decrease of front velocity with time ($v_f = 2c_0 + mt$) (see dotted and dash-dotted lines in Figure 9b). In the experiments, at the beginning, the front position changes as $x_f \sim t^{\alpha}$ with α = 1.8, 1.5, 1, 1.2, 1.1, 1.3 for $\theta = 0°$, 10°, 16°, 19°, 22°, 23.7°, respectively. After a given time, which depends on θ, the flow decelerates more rapidly and $x_f \sim t^{\alpha}$ with α = 0.003, 0.006, 0.42, 0.12, 0.06, 0.4 for $\theta = 0°$, 10°, 16°, 19°, 22°, 23.7°, respectively. Note that in the analytical solution (3), for high inclination angle (i.e., $m \simeq 0$) the flow is roughly described by $x_f \sim t$.

6. Collapse Over Inclined Erodible Bed

[41] In our experiments, the inclination $\theta = 22°$ ($\simeq \theta_r - 2°$) is the highest inclination where a deposit is obtained on the plane with an erodible bed. For $\theta = 23.7°$, the front already clears the end of the flume for an erodible bed of thickness $h_i = 1.4$ mm.

6.1. Flow at Moderate Slope $\theta = 22°$

[42] The presence of an erodible bed significantly affects the dynamics and deposit of granular flows at $\theta = 22°$. Even the presence of a very thin layer of erodible material on the inclined plane increases the runout distance (Figure 10). The maximum distance reached by the avalanche front over a granular layer of thickness $h_i = 4.6$ mm (around six to seven particles) is 40% larger than that obtained on a rigid bed (x_f = 151 cm compared to x_f = 108 cm). For $h_i = 1.82$ mm (around two to three particles) the runout distance (x_f = 119 cm) is still 10% larger than that obtained on a rigid bed.

[43] At the beginning of the experiments ($t < 2\tau_c$), the thickness profile of the flow front seems to be more rounded as the thickness of the erodible bed increases (Figure 10). For $t \leq 5\tau_c$, i.e., until the front reaches the position $x_f = 5.2h_0$ = 73 cm, the position of the front is the same whatever h_i (Figure 11a). After, the mass slowly stretches until a deposit is left on the plane. For $h_i = 4.6$ mm, the final thickness of the deposit is 27% smaller than the thickness obtained for smaller values of h_i for which the final thickness is almost the same (Figure 11b).

[44] Figure 11 shows a first transient acceleration of the mass lasting less than $2\tau_c$, followed by a nearly constant front velocity for about $2\tau_c$. For $t \geq 3 - 4\tau_c$, the front velocity decreases gradually for $h_i < 4.6$ mm until the front stops. For $h_i = 4.6$ mm, two different behaviors are observed: (1) an almost linear decrease of the velocity until about $t \simeq 10\tau_c$ followed by (2) a slower decrease of the velocity until $t \simeq 20\tau_c$. During this second phase, the velocity is about 0.25 m.s^{-1} $\simeq 0.17 v_{\max}$ and $h \simeq 7$ mm in the front zone. It looks like the same change of behavior occurred at $t \simeq 10\tau_c$ for $h_i = 3.38$ mm but lasted only for $2\tau_c$, then coming back to the first regime. Indeed, the presence of an inflexion point around $t \geq 10\tau_c$ reflects the initiation of a slow flow regime after the spreading regime as discussed in the previous section. Interestingly enough, the qualitative behavior of the granular collapse for $\theta = 22°$ and $h_i = 4.6$ mm is very similar to the granular collapse at $\theta = 23.7°$ over a rigid bed involving a first spreading regime followed by a slow flow at almost constant velocity (compare Figures 11c and 9b).

[45] The maximum velocity reached by the front is almost the same whatever the thickness of the erodible bed and is about equal to $v_{\max} = 1.28c_0$ (22°), where c_0 (22°) = $\sqrt{gh_0 \cos\theta}$ = 1.128 m s^{-1} ($v_{\max} \simeq 1.44$ m s^{-1}). At the beginning ($t \leq 2\tau_c$), the front velocity slightly decreases as h_i increases whereas in the main part of the flow, the front velocity increases as h_i increases as was found numerically by *Mangeney et al.* [2007a] in a similar configuration. Similar inversion of the sensitivity to h_i as time changes is observed for the maximum flow thickness (Figure 11b).

[46] The runout distance increases almost linearly with the thickness of the erodible bed h_i (Figure 12a). A stronger variation of the maximum thickness of the deposit h_f and of the time at which the front stops t_f is observed for $h_i \geq 1.5\%$ h_0 (Figures 12b and 12c). The stopping time t_f increases as a function of h_i whereas the final thickness h_f decreases (Figures 12b and 12c). Surprisingly, the functions $r_f(h_i)$, $h_f(h_i)$ and $t_f(h_i)$ look qualitatively similar to the functions $r_f(\theta)$, $h_f(\theta)$ and $t_f(\theta)$ (compare Figures 12 and 7). The mean angle of the deposit on the slope calculated using equation (7) decreases from $\theta_f = 2.3°$ for $h_i = 0$ mm to $\theta_f = 1.2°$ for h_i = 4.6 mm. As a result, the mean angle of the deposit with respect to the horizontal decreases by only 1° from $h_i = 0$ mm to $h_i = 4.6$ mm down to 23.1°.

[47] The stopping phase of the flow is quite different for $h_i = 4.6$ mm compared to the other cases. Indeed, for granular collapse over a rigid bed the front stops before the mass behind it as was observed by *Mangeney-Castelnau et al.* [2005]. Similar behavior seems to occur for $h_i = 1.82$ mm and $h_i = 3.38$ mm. On the contrary, for $h_i = 4.6$ mm, the upper part of the mass stops at $t = 2.08$ s while the front continues to move, until it eventually stops at $t = 2.56$ s.

6.2. Slope Effects on Erosion Efficiency

[48] Experimental results show strong effect of the slope inclination on erosion efficiency (Figures 10, 13, and 14). As

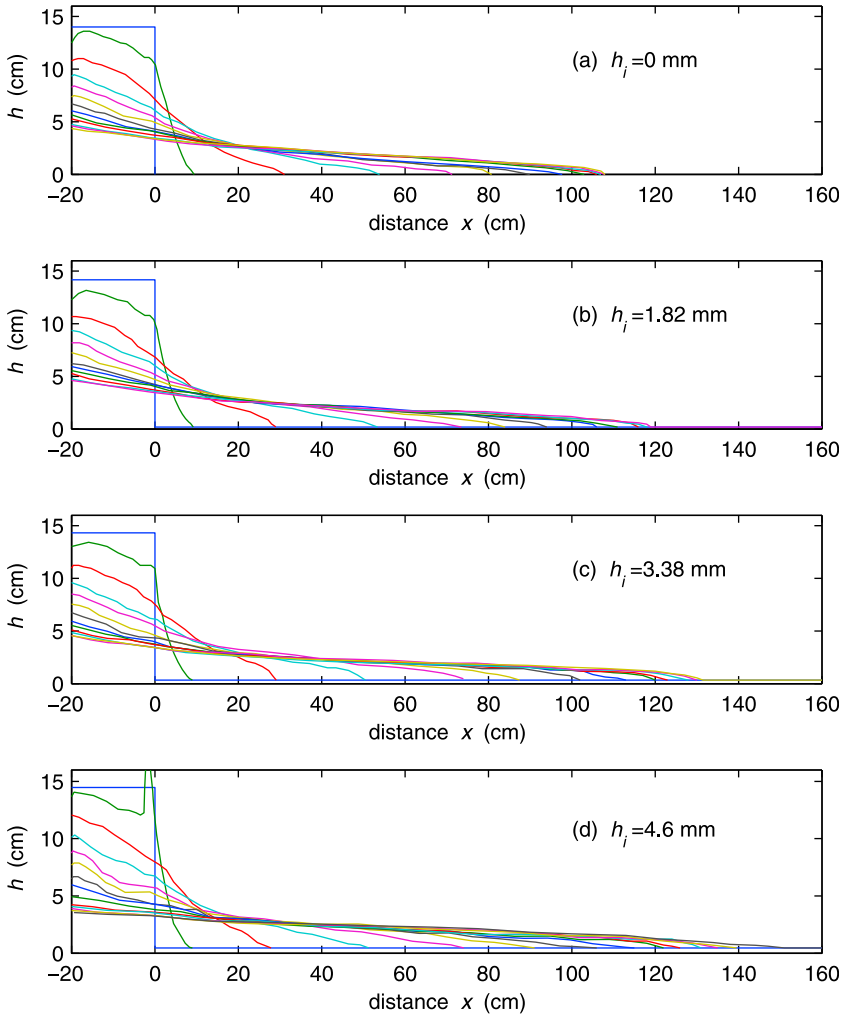

Figure 10. Thickness profile $h(x, t)$ of the granular mass flowing over a plane inclined at $\theta = 22°$ as a function of the down-slope position x over (a) a rigid bed $h_i = 0$ mm, and an erodible bed of thickness (b) $h_i = 1.82$ mm, (c) $h_i = 3.38$ mm, and (d) $h_i = 4.6$ mm. The profiles are represented from time $t = 0$ s to $t = 1.76$ s with $\Delta t = 0.16$ s (Figures 10a and 10b), from time $t = 0$ s to $t = 1.76$ s with $\Delta t = 0.16$ s and at time $t = 1.96$ s (Figure 10c), and from time $t = 0$ s to $t = 1.92$ s with $\Delta t = 0.16$ s and at time $t = 2.56$ s (Figure 10d). These experiments are referred to as E22-j, $j = 0$, 1.82, 3.38, 4.6 in Table 2.

the slope decreases, the flow and the runout distance become less and less affected by the presence of the erodible bed (Figure 15). Eventually, for slope inclination $\theta = 10°$ and $\theta = 0°$, the presence of the erodible bed does not change the runout distance. Experimental results show that the runout distance increases with the thickness of the erodible bed only for inclination angles higher than a critical angle $\theta_c \simeq 12° \simeq \theta_r/2$ which is almost equal here to half of the repose angle of the material.

[49] Interestingly, whatever the inclination angle, the runout distance varies almost linearly with the thickness of the erodible bed (Figure 15). Using equation (5) with the fitted coefficients $k = 0.5$ and $\delta = 27.5°$ leads to the simple relation

$$\frac{r_f}{h_0} = \frac{1}{\tan\delta - \tan\theta} + \gamma(\theta)\frac{h_i}{h_0} \tag{8}$$

with $\gamma(\theta)$ varying from $\gamma(\theta = 0°) = -0.18$ to $\gamma(\theta = 22°) = 0.84$ (insert in Figure 16). The function $\gamma(\theta)$ can be fitted using the empirical relation

$$\gamma(\theta) = \frac{0.02}{\tan 23° - \tan\theta}. \tag{9}$$

For $\theta = 0$, the runout distance slightly decreases as a function of h_i ($\gamma = -0.18$) which is consistent with the numerical results of *Crosta et al.* [2009b] that investigated the effect of the presence of an erodible layer on the collapse of granular column over horizontal bed. Significant decrease of the runout is observed by *Crosta et al.* [2009b] possibly due to the much thicker erodible layer in their case.

[50] Until $t \simeq 2\tau_c$, the front position is quite similar whatever the angle $\theta \geq 16°$ and whatever the thickness of the erodible bed h_i (Figure 16). The influence of the erodible bed can be observed at time $t \simeq 3\tau_c$ for $\theta = 16°$, $t \simeq 4\tau_c$ for

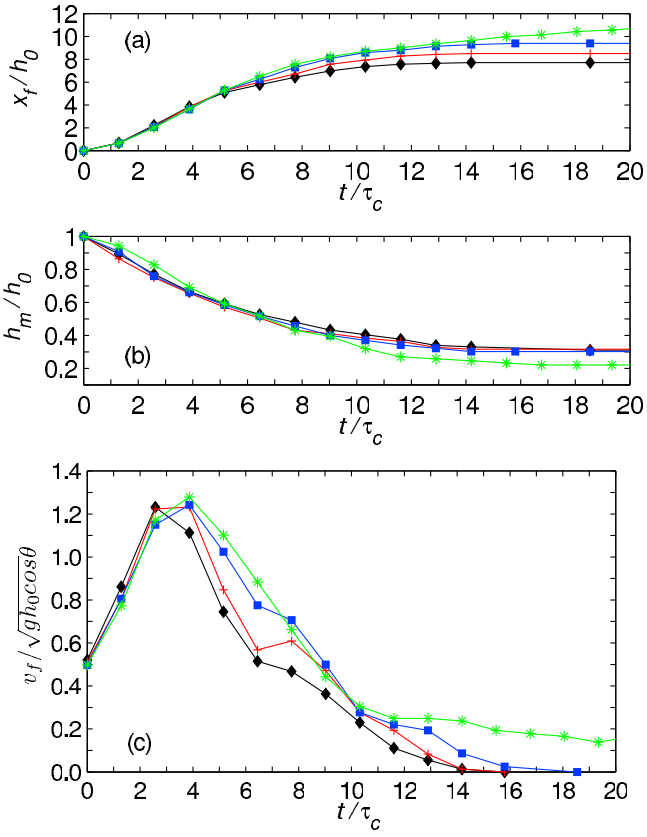

Figure 11. Normalized (a) location of the front x_f/h_0, (b) maximum thickness of the flow (i.e., thickness at the upper wall) h_m/h_0, and (c) velocity of the front $v_f(t)/c_0$ (22°) (c_0 (22°) = $\sqrt{gh_0\cos\theta}$, = 1.128 m.s^{-1}), with h_0 = 0.14 m, as a function of time t/τ_c, where $\tau_c = \sqrt{h_0/(g\cos\theta)}$, = 0.124 s for inclination angle θ = 22° over a rigid bed h_i = 0 (diamond), and erodible bed of thickness h_i = 1.82 mm (cross), h_i = 3.38 mm (square), and h_i = 4.6 mm (star).

θ = 19°, $t \simeq 5\tau_c$ for θ = 22°, and $t \simeq 8.5\tau_c$ for θ = 25.2°. Our results suggest that erosion processes are not efficient during the acceleration phase of the spreading regime discussed in previous sections and start to affect the flow mainly during the following deceleration and slower flow that occurs at sufficient high slopes and/or sufficient thickness of the erodible bed.

[51] Note that a peak is observed for several experiments at the front at the very beginning of the slump (Figure 6c, Figure 10d, Figure 13, and Figure 14) as was also the case for other granular collapse experiments [see, e.g., *Lube et al.*, 2007], due to the initial upward motion of the gate. However, this initial condition seems to weakly affect the flow and the resulting deposit as shown by the very good agreement between this kind of experiments and those carried out by *Siavoshi and Kudrolli* [2005] where the granular mass made of steel beads was released by switching off the magnetic field that initially held the mass.

7. Internal Motion and Wave Propagation

[52] The accuracy of the present experiments did not allow us to make reliable measurements of the flow when the static layer is metastable, i.e., when the layer of the erodible bed is such that $h_i \in [h_s, h_a]$, where h_a is the maximum thickness that can stay on a plane of inclination θ. In this domain, triangular erosion waves propagating at constant velocity downslope have been observed by *Pouliquen and Forterre* [2002], when releasing a 3-D granular cap on an erodible bed. When using here the same granular beads for the released mass and for the erodible bed, the whole bed layer starts flowing at the time the gate unlocks for $h_i \geq h_s(\theta)$. At θ = 25.2°, and with h_i = 3.6 mm ($h_i < h_s$ (25.2°)), the presence of the erodible bed significantly accelerates the flow, but the front does not reach a constant velocity down the plane (Figure 16). Nevertheless, we could build up an erodible bed layer by using black colored particles because these particles had a slightly higher repose angle than the flowing (non colored) regular beads (see section 3). As for the experiments involving regular beads, a substratum of a given constant thickness of black particles was first obtained with a channel slope larger than their repose angle, and then the slope was lowered to run the experiments. For consistency, these experiments were carried out at the same slope angle than those involving a substrate of regular beads (see Table 2), so that the bed of black particles was not strictly metastable owing to the different repose angles of both types of particles.

[53] In the following, we will show some observations of the velocity and general motion within the flowing and the erodible granular layer for θ = 22° and near the metastable regime for $\theta \simeq$ 25° when regular beads are released on an erodible bed made of black beads.

7.1. Internal Velocity and Flowing/Static Interface

[54] The velocity within the flowing mass is measured at the sidewall at inclination angles θ = 22° and θ = 25.4° for flows over an erodible bed of thickness h_i = 5 mm (see section 3 for more details on the velocity measurements). For

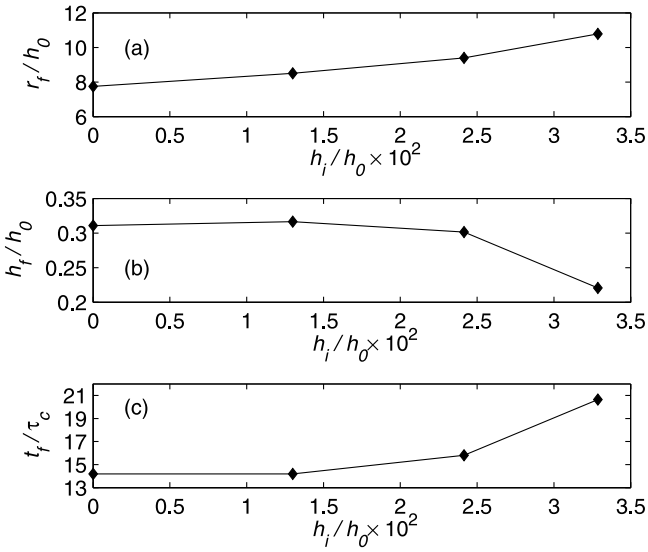

Figure 12. Normalized (a) runout distance r_f/h_0, (b) final thickness at the upper wall h_f/h_0, and (c) time at which the front stops t_f/τ_c where $\tau_c = \sqrt{h_0/(g\cos\theta)}$ = 0.124 s, as a function of the normalized thickness of the erodible bed h_i/h_0 for inclination angle θ = 22°.

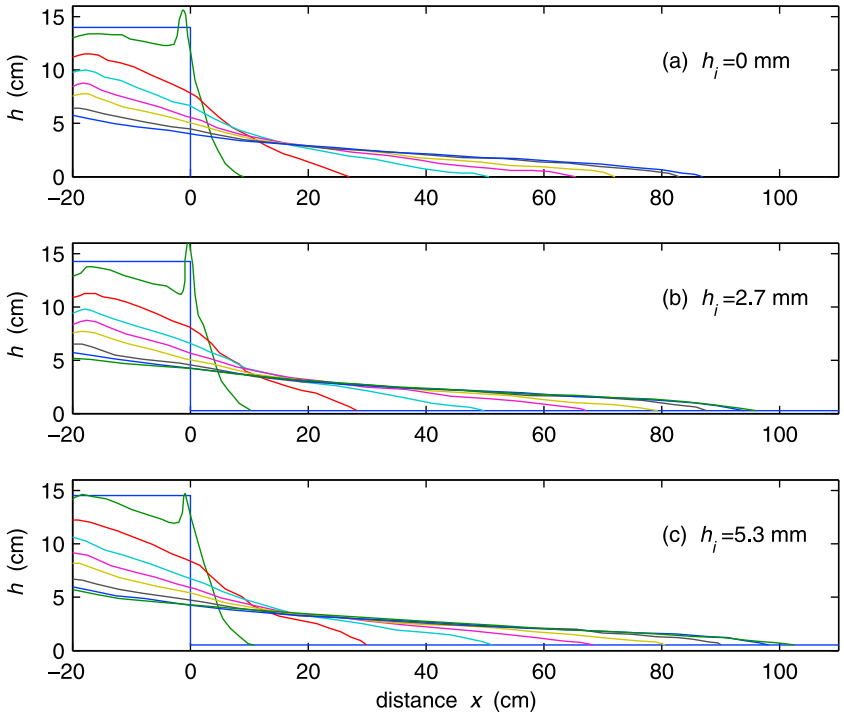

Figure 13. Thickness profile $h(x, t)$ of the granular mass flowing over a plane inclined at $\theta = 19°$ as a function of the down-slope position x over (a) a rigid bed $h_i = 0$ mm at time $t = 0$ s, 0.16 s, 0.32 s, 0.48 s, 0.64 s, 0.8 s, 1.12 s, 1.44 s and an erodible bed of thickness (b) $h_i = 2.7$ mm at time $t = 0$ s, 0.16 s, 0.32 s, 0.48 s, 0.64 s, 0.8 s, 1.12 s, 1.44 s, 1.74 s and (c) $h_i = 5.3$ mm at time $t = 0$ s, 0.16 s, 0.32 s, 0.48 s, 0.64 s, 0.8 s, 1.12 s, 1.44 s, 1.78 s. These experiments are referred to as E19-j, $j = 0$, 2.7, 5.3 in Table 2.

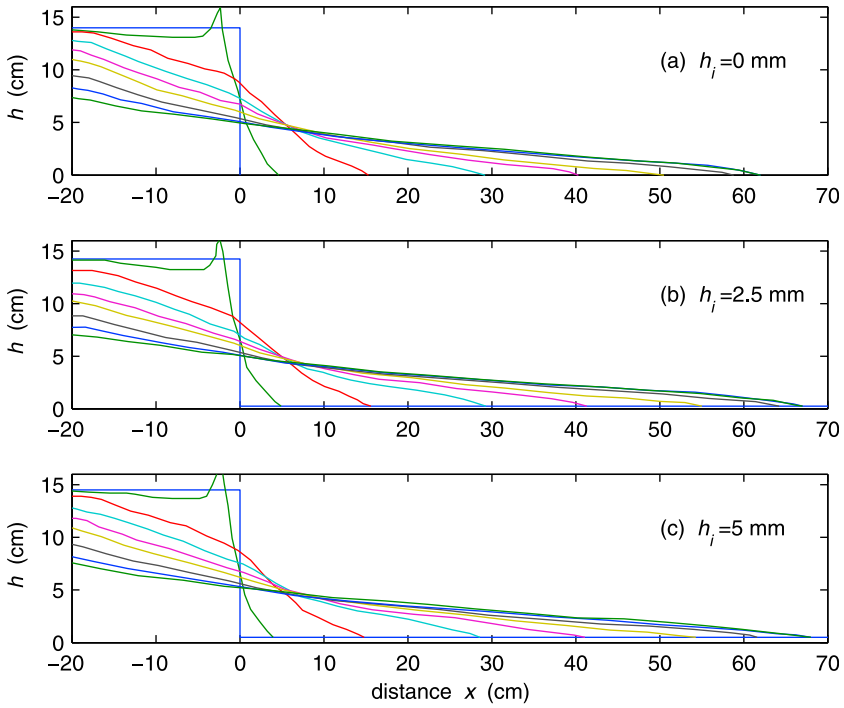

Figure 14. Thickness profile $h(x, t)$ of the granular mass flowing over a plane inclined at $\theta = 16°$ as a function of the down-slope position x over (a) a rigid bed $h_i = 0$ mm at time $t = 0$ s, 0.12 s, 0.24 s, 0.36 s, 0.48 s, 0.6 s, 0.84 s, 1.12 s, 1.62 s and an erodible bed of thickness (b) $h_i = 2.5$ mm at time $t = 0$ s, 0.12 s, 0.24 s, 0.36 s, 0.48 s, 0.6 s, 0.84 s, 1.12 s, 1.6 s and (c) $h_i = 5$ mm at time $t = 0$ s, 0.12 s, 0.24 s, 0.36 s, 0.48 s, 0.6 s, 0.84 s, 1.12 s, 1.52 s. These experiments are referred to as E16-j, $j = 0$, 2.5, 5 in Table 2.

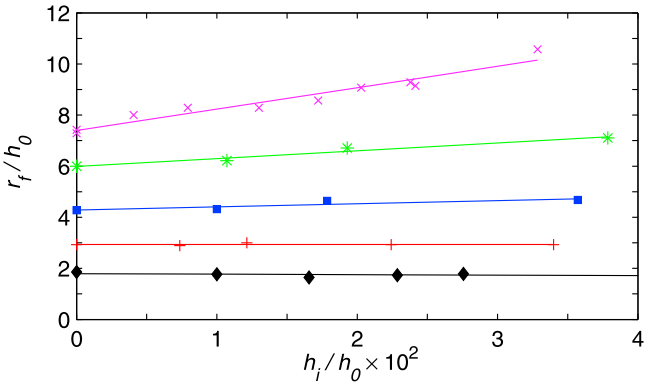

Figure 15. Normalized runout distance r_f/h_0 with h_0 = 0.14 m as a function of the normalized thickness of the erodible bed h_i/h_0 for granular flows over a plane inclined at $\theta = 0°$ (diamond), $\theta = 10°$ (cross), $\theta = 16°$ (square), $\theta = 19°$ (star), and $\theta = 22°$ (times symbol). The size of the symbols reflects the error bar. The full lines correspond to the best linear fit to the data with a slope γ (θ) well fitted by equation (9) (see insert in Figure 16).

$\theta = 22°$, the measurements are performed at $x = 35$ cm, a few tenths of seconds after the front reached this position (i.e., after $t \simeq 0.3$ s). For $\theta = 25.4°$, the measurements are done at $x = 90$ cm and 0.308 s after the front reached this position (i.e., after $t_s = 0.6$ s so that the measurements are done at $t = 0.908$ s). For both $\theta = 22°$ and $\theta = 25.4°$, the velocity profile exhibits a concave shape (Figure 17) similar to that described by *Savage* [1979] and *Ancey* [2002]. For $\theta = 22°$, the method

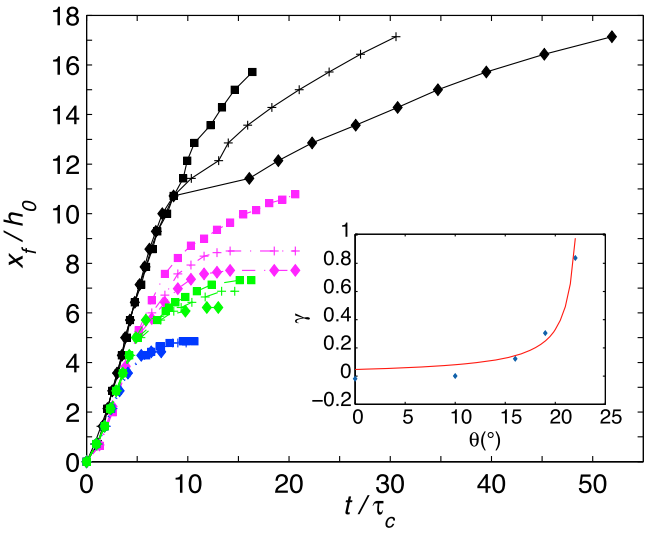

Figure 16. Normalized location of the front x_f/h_0 with h_0 = 0.14 m as a function of time t/τ_c, where $\tau_c = \sqrt{h_0/(g\cos\theta)}$ for inclination angle $\theta = 16°$ (blue dotted lines with diamond for $h_i = 0$ mm, cross for $h_i = 2.5$ mm, and square for $h_i = 5$ mm), for inclination angle $\theta = 19°$ (green dashed lines with diamond for $h_i = 0$ mm, cross for $h_i = 2.7$ mm, and square for $h_i = 5.3$ mm), for inclination angle $\theta = 22°$ (magenta dash-dotted lines with diamond for $h_i = 0$ mm, cross for $h_i = 1.82$ mm, and square for $h_i = 4.6$ mm), for inclination angle $\theta = 25.2°$ (black full lines with diamond for $h_i = 0$ mm, cross for $h_i = 2$ mm, and square for $h_i = 3.6$ mm).

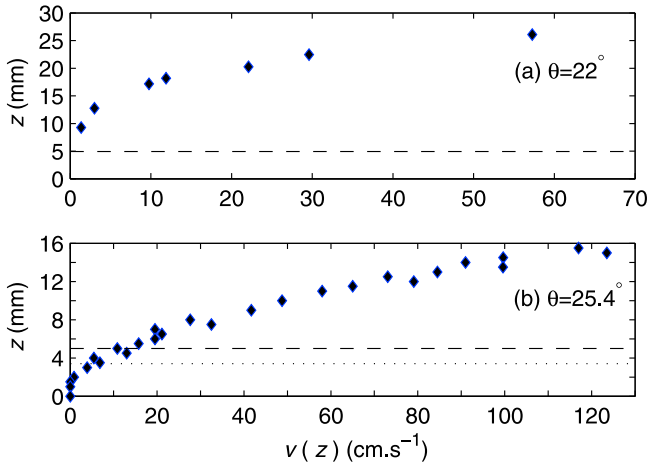

Figure 17. Velocity profile $v(z)$ in cm s^{-1} as a function of z defined as the elevation above the rigid bed for $h_i = 5$ mm and (a) $\theta = 22°$ and (b) $\theta = 25.4°$ (experiments E′22-5 and E′25-5 of Table 2). The velocity is measured at $x = 35$ cm at time $t \simeq 0.4$ s (Figure 17a) and at $x = 90$ cm at time $t - t_s = 0.308$ s (Figure 17b), where $t_s = 0.6$ s corresponds to the time when the front reaches the position $x = 90$ cm. The measurements in Figure 17b are made when the flowing/static interface has reached a maximum depth within the erodible layer (see Figure 18). The position of the top of the erodible bed $z = 5$ mm is shown by dashed lines. The minimum thickness for flow $h_s(25.4°) = 3.4$ mm is added in dotted lines in Figure 17b.

is not precise enough to measure the very small velocity within the erodible bed. For $\theta = 22°$ and $z \geq 14$ mm, the velocity profile is almost linear with mean shear strain rate $\dot{\gamma} = 35s^{-1} = 0.3\sqrt{g/d}$ whereas for $\theta = 25.4°$, the upper almost linear variation of the velocity for $z \geq 4$ mm leads to a shear strain rate $\dot{\gamma} = 95s^{-1} = 0.8\sqrt{g/d}$. An exponential creeping tail is observed below ($z \leq h_s(25.4°) = 3.4$ mm) in agreement with the numerical simulation of *Mangeney et al.* [2007a]. This kind of profile is typical for thin flows over inclined planes or for surface flows on a pile [*GDR MiDi*, 2004; *Forterre and Pouliquen*, 2008; *Siavoshi and Kudrolli*, 2005; *Lube et al.*, 2007].

[55] The measurements at $\theta = 25.4°$ clearly show that the grains within the initially static erodible bed $z \leq 5$ mm are put into motion by the mass flowing over it. A permanent static

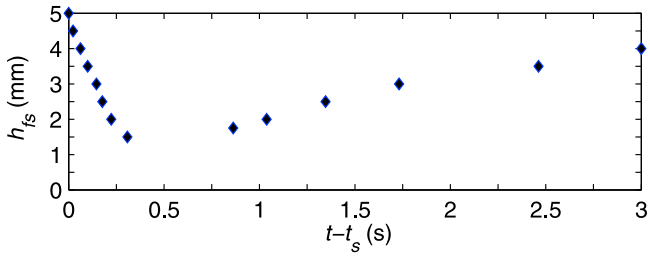

Figure 18. Vertical position of the flowing/static interface within the erodible bed h_{fs} measured at $x = 90$ cm as a function of time $t - t_s$, where $t_s = 0.6$ s corresponds to the time when the front reaches the position $x = 90$ cm for the flow at $\theta = 25.4°$ and $h_i = 5$ mm (experiment E′25-5).

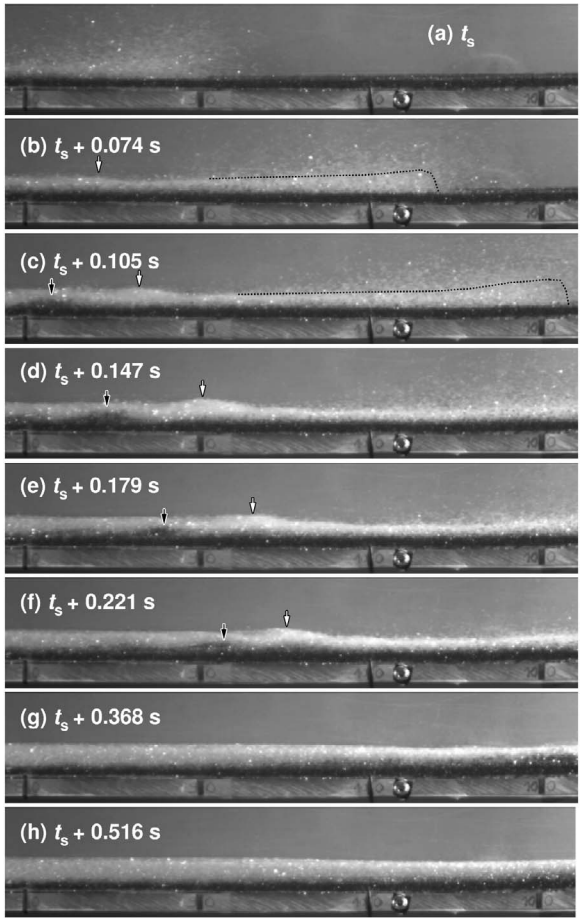

Figure 19. Snapshots at different instants from $t_s = 0.6$ s of the granular mass made of white particles flowing over an erodible bed of thickness $h_i = 3.9$ mm made of black particles at an inclination angle $\theta = 25.2°$. The thick vertical black lines on the rigid substrate measure the position on the plane starting from $x = 80$ cm (first line on the left) indicated every 10 cm. The shape of the front has been roughly outlined in dotted lines in Figures 19b and 19c. White and black arrows are added to the picture to track the position of the crest of a wave observed on the free surface and on the interface between black and white particles, respectively.

layer is still observed for $z \leq 1.5$ mm as shown in Figure 18, where the position of the flowing/static interface h_{fs} is recorded at the same position $x = 90$ cm as the velocity, starting from time $t_s = 0.6$ s at which the front reaches this position. As the front passes the measurement position, the avalanche very rapidly digs into the erodible bed until a maximum penetration depth of 3.5 mm (around 5 grain diameters) is reached after 0.308 s ($2.4\tau_c$). During this period, the penetration depth of the flowing/static interface into the erodible bed increases linearly with time at a vertical velocity $v_{fs} = 1.3$ cm.s^{-1}. Then, the interface stays roughly at this position for about 0.5 s ($4\tau_c$). Eventually, the interface propagates upward during a consolidation phase following an exponential relaxation with a characteristic time $\tau = 2.1$ s. After about 4 s, the flow abandons the flume, leaving a deposit of 4 mm thick on the bed, made mostly of black particles, leading to a total erosion of the bed of about 1 mm all along the slope. The deposit thickness corresponds approximately to $h_s(25.2°)$.

7.2. Wave-Like Motion

[56] A wave-like motion of the flowing/static interface as well as of the free surface of the flow is observed for $\theta = 25.2°$ and $h_i = 3.9$ mm (Figure 19), for $\theta = 25.4°$ and $h_i = 5$ mm (Figure 20) and to a lesser extent for $\theta = 22°$ and $h_i = 3$ mm. For $\theta = 25.4°$ and $h_i = 5$ mm, Figure 20c shows that the flow (and then the deposit) is however quite homogeneous and the thickness of the black layer is about 1 mm smaller than that of the initial erodible bed. On the contrary for $\theta = 25.2°$ and $h_i = 3.9$ mm, the final thickness of the black layer is approximately the same as that of the initial erodible bed, even though significant waves propagated during the flow. As a result, the thickness of the black layer once the flow has stabilized almost corresponds to the thickness of the deposit left on the plane $\sim h_s(\theta)$, whatever the value of h_i.

[57] Figure 19 shows a saltating front of white particles including some black particles. Behind the saltating front,

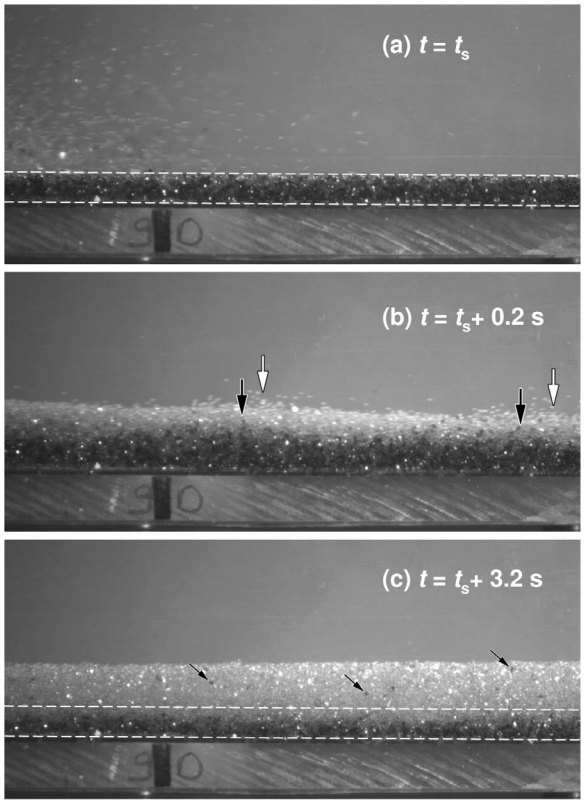

Figure 20. Snapshots of the granular mass made of white particles flowing over an erodible bed of thickness $h_i = 5$ mm made of black particles at inclination angle $\theta = 25.4°$ at (a) $t_s = 0.6$ s, (b) $t = 0.8$ s, and (c) $t = 3.8$ s. The initial position of the erodible bed is outlined using two dashed parallel white lines in Figures 20a and 20c. The thick vertical black line indicates the position along the plane ($x = 90$ cm). White and black arrows are added to the picture to track the position of the crest of a wave observed on the free surface and on the interface between black and white particles, respectively. In Figure 20c, inclined arrows point out some black particles carried away by the flow.

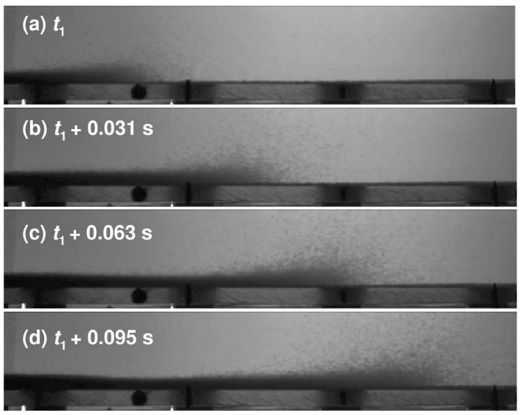

Figure 21. Snapshots of the front zone from time t_1 when the front crosses the position $x = 77$ cm taken every 0.031 ± 0.001 s in the region $x \in [70, 100]$ cm from the gate for granular collapse over a rigid bed ($h_i = 0$ mm) at $\theta = 25.2°$. The front has a steep shape when saltating grains are not taken into account.

undulations of the free surface and of the black layer of initially static particles can be observed with comparable wavelength, but a phase shift (Figures 19c–19f). These waves seem to make the black particles rise toward the free surface, causing some mixing of white and black particles. Some white particles can be found within the bottom black layer as well as black particles within the flow and deposit (Figures 19 and 20c). This mixing layer is seen 2 mm above and under the initial elevation of the erodible layer for $\theta = 25.4°$ and $h_i = 5$ mm. Qualitatively similar behavior is observed for $\theta = 22°$ and $h_i = 3$ mm. In that case, the mixing occurs within a layer about 1 mm thick near the upper elevation of the erodible bed.

[58] The waves seem to be located behind the front. Indeed, at the position $x = 90$ cm, the wave motion lasts about 0.3 s after the front passes (Figure 19). Interestingly, this time corresponds to the time of maximum penetration of the flowing/static interface within the erodible bed. At time $t \simeq 0.5$ s, the flow stabilizes in the whole domain captured by the camera (80 cm $\leq x \leq$ 110 cm), while the free surface still exhibits smooth oscillation with a larger wavelength. Our results suggest that these waves play a key role in the erosion efficiency in the zone near the front. Similarly, for $\theta = 22°$, the wavy motion ceases after the elapsed time $\Delta t \simeq 0.2$ s counted from the moment the front passes this position. Note that waves are also observed behind the front for flow over a rigid bed at inclination angles $\theta \simeq 25°$ (Figure 21). These waves could result from the irregularities of the rigid bed or from flow instability.

[59] By following the maximum amplitude of the oscillations, a wave propagation speed can be estimated. The wave speed is about 0.75 m.s^{-1} $\simeq 0.7c_0$ (25.2°) for $\theta = 25.2°$ and $h_i = 3.9$ mm and 0.45 m.s^{-1} $\simeq 0.4c_0$ (22°) for $\theta = 22°$ and $h_i = 3$ mm. For $\theta = 22°$, the wave speed is calculated in between times $t = 0.398$ s ($3\tau_c$) and $t = 0.457$ s ($3.7\tau_c$) which corresponds to the "steady" maximum velocity of the front $v_f \simeq 1.2c_0 = 1.35$ m.s^{-1} (see Figure 11c). As a result, the wave speed is about 3 times smaller than the front velocity at this instant. Note that for $\theta = 25.2°$ and $h_i = 3.9$ mm the wave speed calculated from snapshots taken between times 0.747 s and 0.895 s ($\Delta t \simeq 1.2\tau_c$) is almost constant during this period (Figures 19b–19f).

7.3. Steep Fronts

[60] It is difficult to define the profile of the front due to strong saltation effects (Figures 19a–19c and 21). Individual beads can reach altitudes up to 10 cm above the rigid bed. Nevertheless, at inclination angle $\theta \simeq 25°$, it looks like the front has a steep, blunt shape whatever the value of h_i (Figures 19 and 21). No steep fronts are observed at $\theta = 22°$.

[61] For a granular collapse over an erodible bed at $\theta = 25.2°$, the blunt nose extends over about 20 cm along the plane as shown in Figure 19c. The maximum flow thickness above the rigid bed near the front is about 15 mm ($h/h_s \equiv 4$, i.e., about 22 particles). For flow over a rigid bed, the steep front has about the same dimensions (Figure 21d). As a result, the steep, wave-like fronts obtained here are not specifically related to erosion processes, contrary to the triangular front observed by *Pouliquen and Forterre* [2002] for granular flows of similar glass beads at $\theta = 23°$. Furthermore, the dimensions of our front zone are quite different from the dimensions of theirs, which extended 40 cm down the plane with a maximum thickness of $h/h_s \equiv 0.7$ above the erodible bed. Note that 3-D triangular fronts were also obtained by *Börzsönyi et al.* [2008] for avalanches made of glass beads similar to our beads, flowing over an erodible bed at inclination $\theta = 24.3°$. In their experiments, the avalanches were generated by a constant supply on top of the plane. In that case, the observed front has a typical length of 22 cm down the slope and maximum thickness of $h/h_s \simeq 1.5$ which is closer to our observations.

[62] One explanation of these observations may be that steep fronts are generated during the slow flow that follows the spreading regime. The steep front will then appear when the slow regime starts to be important: either for flows over a rigid substrate when increasing the inclination angle or at a given inclination angle when increasing the thickness of the erodible bed (see Figures 9b and 11c).

8. Discussion

[63] Part of our results can be easily understood by referring to the properties of granular flows. When a granular avalanche flows over an erodible bed, the initially static material can be put into motion by the flowing mass. This process is associated with energy exchange between the flowing and static masses. The kinetic energy of the flowing mass is consumed to put into motion static material, while the kinetic energy of the flowing mass is increased in turn by the addition of flowing grains. In other words, the potential energy of the static grains is converted into kinetic energy [*Mangeney et al.*, 2007a]. The more stable the static grains are, the more energy is required to put them into motion. Obviously, a given layer of granular material is more stable at a small inclination angle than on steep slopes. More specifically, a granular layer lying on an horizontal bed is always stable whatever its thickness. On the contrary, in a range of inclination angles around the repose and avalanche angles of the material ($\theta \in [\theta_r, \theta_a]$), a granular layer could either be stable or unstable depending on its thickness [*Pouliquen*, 1999; *Daerr and Douady*, 1999]. Furthermore, in this range of inclinations, an initially static layer can be destabilized by a small perturbation. It is there-

fore very natural to observe higher efficiency of erosion processes when the slope increases.

[64] In contrast, the origin of the critical value of the angle above which erosion starts to affect the flow (which in our specific experiments corresponds to $\theta_c \simeq \theta_r/2$) is more difficult to understand. The use of material with different friction angles may challenge the link of the critical angle to the repose angle of the material. Furthermore, as our experiments are performed using a single geometry of the initial released mass, it is possible that this critical value of the inclination angle depends on the initial conditions.

[65] The angle θ_c seems to separate two types of behavior of the flow: for $\theta \leq \theta_c$, only a spreading regime is observed that is qualitatively similar to granular collapse over a horizontal bed, with an acceleration phase followed by a deceleration. On the other hand, for $\theta > \theta_c$, the decelerating phase after the initial acceleration departs from the quasi-symmetric bell-shape of the front velocity observed during the spreading regime over horizontal bed (Figure 9b). A slow thin flow tends to develop. Erosion only affects the flow in the decelerating phase and in the slow flow. One can suspect that during the accelerating phase ($t < 4\tau_c$) the longitudinal pressure gradients play a key role by pushing the mass down the slope. Whatever the thickness of the erodible bed, the front is essentially driven over it by a pressure gradient that does not change significantly when adding a few particles on the plane. On the contrary during the decelerating phase, the granular mass is much flatter. Thus, in the slow regime, the front chooses its own dynamics depending on gravity, friction and availability of mass.

[66] Although the velocity is much smaller during the slow flow following spreading, experimental results suggest that erosion strongly changes the front velocity during this regime. One possible explanation is that during the spreading regime, the grains from the erodible bed that are put into motion rapidly decelerate, so that the flow does not make the most of the energy lost in extracting them from the bed. Actually, a time delay is expected to occur before the extracted grains are accelerated up to the flow speed. On the contrary during the slow regime, while the velocity is small, it decreases less rapidly with time making it possible to increase the kinetic energy over a longer period.

[67] Our results suggest that the front zone (about 50 cm behind the front) plays a key role in the erosion processes. The rapid penetration of the flowing/static interface in the erodible layer behind the front and its further stabilization at a given elevation, slightly smaller than $h_s(\theta)$, are in very good agreement with the numerical prediction of *Mangeney et al.* [2007a, Figure 2] using the partial fluidization model developed by *Aranson and Tsimring* [2002] and *Aranson et al.* [2008]. This continuum model is based on an explicit description of the flowing/static transition in granular flow borrowed from the Ginzburg-Landau theory of phase transition. As numerical simulations reproduce qualitatively much of the experimental observations but do not show any waves propagating at the free surface nor at the flowing/static interface, it could be possible that these waves are not a necessary ingredient to explain the main physical processes acting in our experiments. However, the waves may help to extract the grains from their place in the geometrical arrangement of the layer and from the friction force exerted by the neighboring grains. Actually, these waves induce a vertical motion pushing the grains toward the surface and making them join the flow.

[68] Steep bulbous front waves propagating at almost constant velocity are observed at high inclination ($\theta = 25.2°$), i.e., in the metastable regime, for flows over both a rigid and an erodible bed (Figures 19a, 19b, 19c, and 21). Similar waves with a more triangular shape have been previously observed and simulated for granular flows on erodible beds. Erosion processes have been thought to be at the origin of wave generation. Although the dimensions of the wave observed here are slightly different from those found in the former studies, our results suggest that generation of steep front waves could also be obtained for flows over a rigid bed with increasing inclination angle. Our experimental results suggest that increase of slope and increase of the thickness of the erodible layer act in a similar way on the flow dynamics and on the potential of surge generation as if the energy gained by the additional flowing grains were to add to the gravitational energy compensating the energy lost by friction.

[69] It is tempting to try understanding the steep front waves observed for granular flows over erodible beds by using simple thin layer models of granular flows over a thin layer made of the same material. An analytical solution of sloping dam-break of frictional material over an erodible bed has been therefore developed here (see Appendix A). In that case, a shock develops at the front of the flow. The analytical solution shows that the velocity of the front decreases as h_i increases which is the opposite of what is observed here (Figure A2 in Appendix A). Simple thin layer granular models are thus expected to fail in reproducing the increase of mobility for increasing thickness of the erodible layer, suggesting that an explicit description of the flowing/static transition in granular flows has to be taken into account.

[70] Despite the oversimplification of erosion processes in our experiments with respect to natural situations, the results can be compared to some field observations. In our experiments for $\theta \in [22°, 25°]$ the flowing/static interface penetrates at 0.1–0.35 cm within the erodible bed for typical flow thickness near the front of about 0.7–1 cm leading to penetration depth of 0.1–0.5 times the thickness of the flowing lobe. On Lascar volcano, *Sparks et al.* [1997] report typical thickness of pyroclastic deposit lobes near the front ranging from 0.2 to 1 m as well as erosional furrows 0.1–0.3 m deep observed on slopes of the order of 20°. Thus the erosion depth is 0.3–0.5 times the thickness of the flowing lobe. This is also comparable with observation of debris flows in the French Alps where the flow thickness approximated by the thickness of the levees is about 3 m and the erosion depth about 1 m (Figure 2). Our simple experiments are in agreement with the observations of *Sparks et al.* [1997] showing that the topography and availability of loose surface material are among the most important controls on erosion in the Lascar pyroclastic flows. Our experimental results show a vertical motion of beads generated by the internal waves propagating within the flow that could be compared to the evidence of particle mixing in these pyroclastic flows. Finally, *Sovilla and Bartelt* [2002] observed that the maximum flow heights of snow avalanches are generally located considerably behind the front. However, when the avalanche runs on a steep track (35°–40° in their case), the maximum heights move forward,

closer to the avalanche front. These results support our observation that avalanches tend to develop steep fronts at high inclination angles.

[71] The significant impact of erosion on the mobility of granular material makes it necessary to include these processes in natural flow modeling especially for improving hazard prediction [e.g., *Hungr and Evans*, 2004; *Mangeney et al.*, 2007b; *Pirulli and Mangeney*, 2008; *Pirulli et al.*, 2007; *Bouchut et al.*, 2008; *Fernandez-Nieto et al.*, 2008; *Heinrich et al.*, 1999; *Pudasaini and Hutter*, 2007; *Crosta et al.*, 2009a, 2009b; *Kuo et al.*, 2009; *Mangold et al.*, 2010; M. Pastor et al., A SPH depth integrated model with pore pressure coupling for fast landslides and related phenomena, paper presented at 2007 International Forum on Landslide Disaster Management, Hong Kong Geotech. Soc., Hong Kong, 10–12 December 2007]. Discrete element models are expected to successfully describe erosion processes in simple configurations such as the experiments performed here [e.g., *Deboeuf et al.*, 2005], but their present computational cost is too high for application to geological flows because of the shape and size distribution of natural material. Indeed, properties of avalanches and especially erosion waves depend dramatically on the shape (spherical or irregular) of the grains [*Börzsönyi et al.*, 2008]. Avalanches formed of sand particles are larger than avalanches formed of glass beads. It is thus expected that the complex shapes of natural granular material may lead to greater waves compared to the erosion waves obtained with regular particles as those used here. On the other hand, the explicit description of erosion processes in continuum models is still a challenge because of the lack of theoretical understanding of the flowing/static transition in granular material [e.g., *Chen et al.*, 2006; *Jop et al.*, 2006; *Mangeney et al.*, 2007a; *Doyle et al.*, 2007; *Pudasaini and Hutter*, 2007; *Bouchut et al.*, 2008; *Tai and Kuo*, 2008; *Crosta et al.*, 2009a].

9. Conclusion

[72] Experiments of granular collapse over rigid and erodible inclined beds have been performed in order to better understand and quantify erosion processes observed in natural flows. We focus here on the effects of the slope and of the thickness of the erodible layer on flow dynamics and morphology of the deposits. The main results of our study are as follows:

[73] 1. Granular collapse deposits over inclined rigid bed are well described by simple functions of the parameter $\Delta = \tan\theta - \tan\delta$, where θ is the inclination angle of the plane and δ the friction angle of the material involved.

[74] 2. Erosion processes strongly affect the dynamics and runout (i.e., mobility) of granular flows over sloping beds. Increase of 40% of the runout distance is observed on moderate slopes, i.e., close to the repose angle of the grains, even for very small thickness of the erodible layer.

[75] 3. Erosion efficiency strongly increases as the slope increases. There is a critical slope θ_c, here about half the repose angle of the granular material, over which erosion starts to affect the flow. For gentler slopes, the flow and deposit are insensitive to the presence of an erodible layer. Whatever the slope $\theta \geq \theta_c$, the runout distance increases almost linearly with the thickness of the erodible bed, suggesting that erosion efficiency is mainly supply-dependent.

[76] 4. Two flow regimes are observed for granular collapse: a first spreading phase with high maximum velocity, followed by a slow flowing phase. The slow thin flow is observed only if the slope is high enough ($\theta \geq \theta_c$) and its duration significantly increases with increase of the slope or of the thickness of the erodible layer. Erosion affects the flow mainly during the decelerating phase and the second slow regime, possibly explaining the critical slope for which erosion starts to play a role.

[77] 5. Measurements of velocity profile within the flow show that grains from the erodible bed are put into motion by the upper flow. The penetration depth of the flowing/static interface into the erodible layer rapidly increases behind the front of the granular mass, stabilizing at a constant value and then rising following an exponential function toward the elevation $z \simeq h_s(\theta)$ above the rigid bed (here h_s is the minimum thickness of the granular layer that can flow on the plane).

[78] 6. Waves are observed both on the free surface and on the flowing/static interface. These waves seem to play a key role in erosion efficiency by inducing a vertical motion that removes grains from the erodible bed toward the surface, allowing them to be caught up by the flow. These waves mainly propagate within a zone extending about 50 cm behind the front, underlining the major role of frontal erosion.

[79] 7. Steep fronts are observed at high inclination angles, regardless of the presence of an erodible bed. These result from yet unknown physical processes (bed irregularities, flow instability, …).

[80] 8. Simple scaling laws have been deduced from the experimental results, making it possible to give a first quantitative estimation of the deposit morphology (runout distance, maximum thickness) and of the emplacement time for a given inclination angle and a given thickness of erodible material. The friction angle of the material appears to be equal to the mean angle of the deposit that can be measured on the field.

[81] These results are consistent with some field observations and provide a first systematic study of erosion processes as a function of the slope and of the supply of the erodible material, at least for the very simple situation investigated here. Much more work has to be performed to investigate the effect on erosion efficiency of the initial shape and volume of the released mass or of the nature of the substrate (shape and frictional properties of the grains, cohesive material, presence of a fluid phase, etc…). Rapid variation of the topography may also play a significant role, while favoring flow instability and possibly reinforcing wave generation within the flow that appears to increase erosion efficiency.

[82] Erosion processes are shown to be an essential ingredient of granular flow dynamics that have to be taken into account in natural flow modeling. As the description of erosion processes related to the flowing/static transition in granular material is still a challenge for the community, these results provide quantitative measurements that can help constrain theoretical and numerical models.

Appendix A: Analytical Solution for Inclined Frictional Dam Break Over a Granular Bed

[83] We present here the analytical solution of a dam break problem that describes the flow of a frictional material over a sloping plane covered by a thin layer made of the same

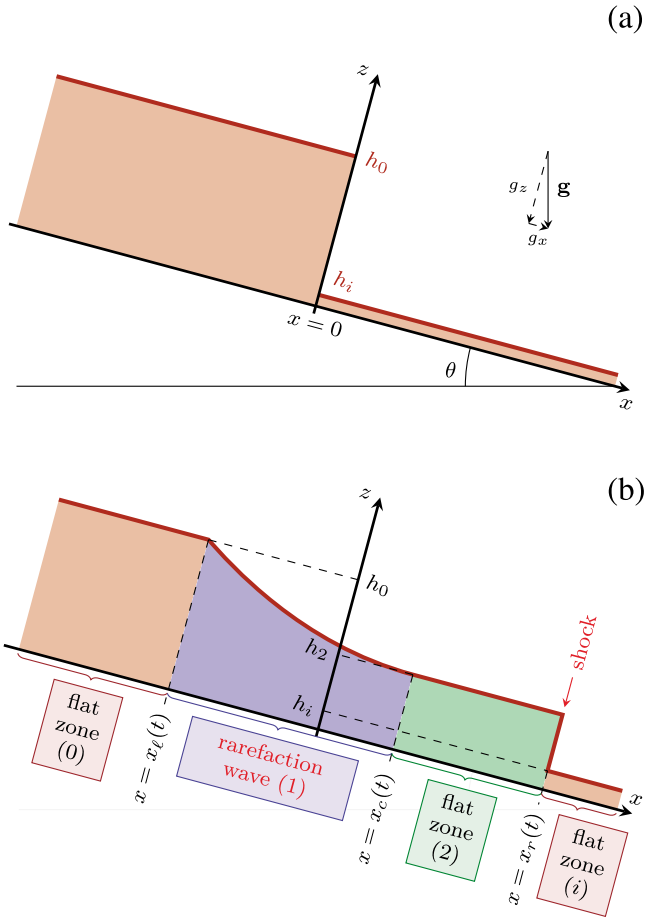

Figure A1. Dam break problem: free surface at (a) $t = 0$, and (b) $t > 0$.

material. We consider the simple case of an uniform slope inclined at an angle θ, higher than the friction angle δ.

[84] The coordinate system is linked to the topography, i.e., x and z axes are parallel and perpendicular to the uniform slope, respectively. A simple representation of the material flow is described by the mass and momentum conservation equations that can be written as

$$\begin{cases} \partial_t h + \partial_x(hu) = 0, \\ \partial_t(hu) + \partial_x(hu^2 + g_z h/2) = mh, \end{cases}$$

where $h \equiv h(x, t) \geq 0$ is the material thickness, $u \equiv u(x, t)$ is the depth-averaged horizontal velocity, $g_z = -g\cos\theta < 0$ is the z component of the acceleration due to gravity, and $m = g_x + F \geq 0$ is the constant x acceleration resulting from the sum of the acceleration due to gravity $g_x = g\sin\theta$ and the well-known Coulomb-type frictional law $F = -g_z \tan\delta$ (see section 4 and *Mangeney et al.* [2000, 2003, 2007b] for more details on the model). The material is released from rest at the initial instant and the initial conditions are those of a dam of constant depth and infinite length in the upslope x direction (see Figure A1a):

$$h(x, t = 0) = \begin{cases} h_0 & \text{if } x < 0, \\ h_i & \text{if } x > 0, \end{cases}$$
$$u(x, t = 0) = 0 \text{ for all } x \in \mathbb{R},$$

with $h_0 > h_i > 0$ (see Figure A1a).

[85] The analytic hydrodynamic solution of this problem is composed of three flat zones: the two original inactive zones (0) and (i) at the two ends and an intermediate zone (2) connected on the left flat zone by a rarefaction wave (1) and on the right flat zone by a shock wave (see Figure A1b). Using $c_i \equiv \sqrt{g_z h_i}$ and $c_j \equiv \sqrt{g_z h_j}$ for $j = 0, 1, 2$, we can parameterize

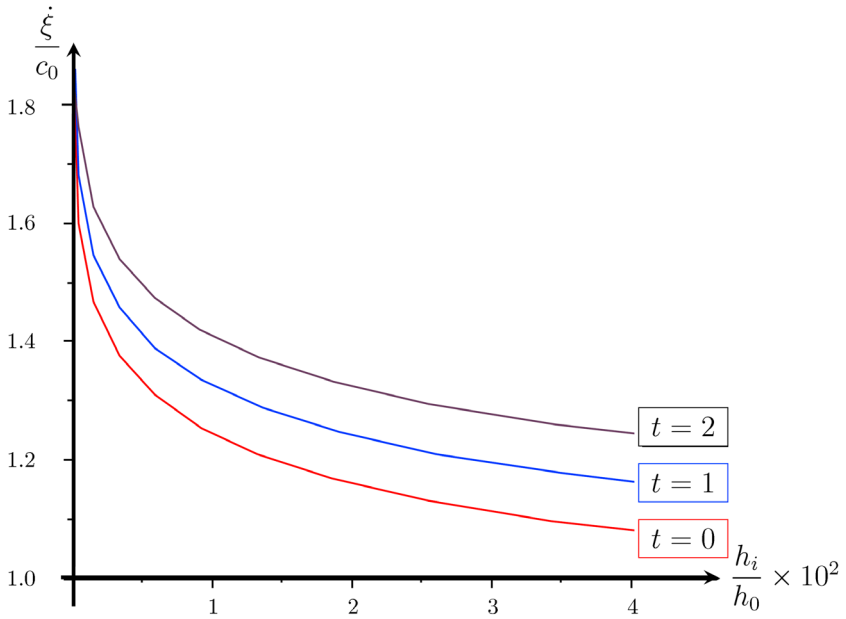

Figure A2. Normalized speed of the shock $\dot{\xi}/c_0$ located at the front of the flow as a function of the normalized thickness of the erodible layer h_i/h_0, for $h_0 = 0.14$ m, $\theta = 22°$, and $\Delta = 21.5°$, at different times.

the evolution of the free surface $h(x, t)$ and the velocity $u(x, t)$ by the ratio $k \equiv \sqrt{h_0/h_i} = c_0/c_i > 1$ as follows:

$$h(x,t) = \begin{cases} h_0 & \text{if } x \le x_\ell(t), \\ h_1(x,t) = \dfrac{1}{9g_z}\left(2c_0 + \dfrac{mt}{2} - \dfrac{x}{t}\right)^2 & \text{if } x_\ell(t) \le x \le x_c(t), \\ h_2(x,t) & \text{if } x_c(t) \le x < x_r(t), \\ h_i & \text{if } x > x_r(t), \end{cases}$$

$$u(x,t) = \begin{cases} u_0(t) = mt & \text{if } x \le x_\ell(t), \\ u_1(x,t) = \dfrac{2}{3}\left(c_0 + mt + \dfrac{x}{t}\right) & \text{if } x_\ell(t) \le x \le x_c(t), \\ u_2(x,t) & \text{if } x_c(t) \le x < x_r(t), \\ u_i(t) = mt & \text{if } x > x_r(t), \end{cases}$$

with $x_\ell(t) = -c_0 t + mt^2/2$, $x_c(t) = (2c_0 - 3c_2)t + mt^2/2$ and $x_r(t) = \dot{\xi}t$, where $\dot{\xi}$ is the shock speed. The states u_2 and c_2 (then also h_2) are connected to $\dot{\xi}$ by the following relations:

$$c_2 = c_i\sqrt{-\frac{1}{2} + \frac{1}{2}\sqrt{1+8\eta^2}},$$

$$u_2 = \left[\eta - \frac{1}{4\eta}\left(1 + \sqrt{1+8\eta^2}\right)\right]c_i + u_i,$$

while $\eta = (\dot{\xi} - u_i)/c_i$ is a function of k. We underline that $(u_2 - u_i)/c_i$ and c_2/c_i (then also h_2/h_i) depend only on η. The complete solution $h(x, t)$ and $u(x, t)$ is obtained by computing η as a function of the ratio k by solving the following nonlinear equation:

$$\eta - \frac{1+\sqrt{1+8\eta^2}}{4\eta} + 2\sqrt{\frac{-1+\sqrt{1+8\eta^2}}{2}} = 2k.$$

We note that if $h_i = 0$ we get the solution described by *Mangeney et al.* [2000], if $\theta = \delta = 0$ (then $m = 0$) we get the solution developed by *Stoker* [1957], and if $h_i = \theta = \delta = 0$ (then $m = 0$) we get the solution of *Ritter* [1892].

[86] We were not able to find any explicit expression for $\eta = \eta(k)$. However, a simple mathematical study shows that η is a single-valued function of k with a monotone decrease as h_i/h_0 increases.

[87] Solving numerically this equation for a discrete set of k values for $k > 1$ shows that $\dot{\xi}/c_0(t)$ always decreases as h_i/h_0 increases at a given time (see Figure A2) contrary to what is observed in the experiments presented here. Indeed, Figure 11c shows that at a given time $t \ge 4\tau_c$, the front velocity v_f increases as h_i increases while for smaller values of t the front velocity is almost constant whatever h_i.

Notation

θ	Inclination angle of the plane
θ_r, θ_a	Repose and avalanche angles of the glass beads
d, ρ, ν	Diameter of the beads, and density and porosity of the granular material
x, z	Coordinates in the downslope direction and in the direction perpendicular to the slope
h_0, r_0, a	Initial thickness, downslope extension, and aspect ratio of the released mass
h_i	Initial thickness of the erodible bed
h_f, r_f, θ_f	Final thickness, runout distance, and mean angle of the deposit
t_f	Time at which the front stops
$x_f(t)$, $v_f(t)$	Front position and front velocity
$h_m(t)$	Maximum thickness of the flow
$v(z)$	Vertical profile of the horizontal velocity at a given position along the plane
$h_s(\theta)$	Minimum thickness of flow at a given angle θ
α, δ_1, δ, k, γ, β	Empirical parameters in the scaling laws
g	gravity
c_0, m	Wave velocity in thin layer granular flows, variable of the analytical solution
τ_c	Characteristic time
θ_c	Critical angle for the efficiency of erosion effects
$h_{fs}(t)$	Position of the interface between flowing and static grains
t_s	Time at which the front reaches a given position along the slope
$\dot{\gamma}$	Strain rate

[88] **Acknowledgments.** We thank Agathe Bucherie for the initiation of this work during her Master's degree training. We are grateful to Christophe Ancey and two anonymous reviewers for their interesting comments. This work was supported by the Agence Nationale de la Recherche ANR VOLBIFLOW, ANR PLANETEROS and ANR UNDERVOLC. Contribution IPGP 3040.

References

Ancey, C. (2002), Dry granular flow down an inclined channel: Experimental investigations on the frictional-collisional regime, *Phys. Rev. E*, *65*, 011304.

Ancey, C. (2004), Powder-snow avalanches: Approximation as non-Boussinesq clouds with a Richardson-number-dependent entrainment function, *J. Geophys. Res.*, *109*, F01005, doi:10.1029/2003JF000052.

Ancey, C., R. M. Iverson, M. Rentschler, and R. P. Denlinger (2008), An exact solution for ideal dam-break floods on steep slopes, *Water Resour. Res.*, *44*, W01430, doi:10.1029/2007WR006353.

Aranson, I. S., and L. S. Tsimring (2002), Continuum theory of partially fluidized granular flows, *Phys. Rev. E*, *65*, 061303.

Aranson, I. S., F. Malloggi, and E. Clement (2006), Transverse instability in granular flow down an incline *Phys. Rev. E*, *73*, 050302.

Aranson, I. S., F. Malloggi, E. Clement, and L. S. Tsimring (2008), Nonlocal rheological properties of granular flows near a jamming limit, *Phys. Rev. E*, *78*, 031303.

Balmforth, N. J., and R. R. Kerswell (2005), Granular collapse in two dimensions, *J. Fluid Mech.*, *538*, 399–428.

Benda, L. (1990), The influence of debris flows on channels and valley floors in the Oregon Coast Range, U.S.A., *Earth Surf. Proc. Landforms*, *15*, 457–466.

Berti, M., R. Genevois, R. LaHusen, A. Simoni, and P. R. Tecca (2000), Debris flow monitoring in the Acquabona Watershed on the Dolomites (Italian Alps), *Phys. Chem. Earth, Part B*, *25*(9), 707–715.

Bonnard, C., L. Laloui, C. Scavia, and M. Castelli (Eds.) (2009), The mechanics and velocity of large landslides, *Eng. Geol.*, *109*, 1–160.

Börzsönyi, T., T. C. Halsey, and R. E. Ecke (2005), Two scenarios for avalanche dynamics in inclined granular layers, *Phys. Rev. Lett.*, *94*, 208001.

Börzsönyi, T., T. C. Halsey, and R. E. Ecke (2008), Avalanche dynamics on a rough inclined plane *Phys. Rev. E*, *78*, 011306.

Bouchut, F., E. Fernandez-Nieto, A. Mangeney, and P. Y. Lagre (2008), On new erosion models of Savage-Hutter type for avalanches, *Acta Mech.*, *199*(1–4), 198–208.

Calder, E. S., R. S. J. Sparks, and M. C. Gardeweg (2000), Erosion, transport and segregation of pumice and lithic clasts in pyroclastic flows inferred from ignimbrite at Lascar Volcano, Chile, *J. Volcanol. Geotherm. Res.*, *104*, 201–235.

Chen, H., G. B. Crosta, and C. F. Lee (2006), Erosion effects on runout of fast landslides, debris flows and avalanches: A numerical investigation, *Geotechnique*, *56*(5), 305–322.

Crosta, G. B., S. Imposimato, and D. Roddeman (2009a), Numerical modeling entrainment/deposition in rock and debris-avalanches, *Eng. Geol.*, *109*, 135–145.

Crosta, G. B., S. Imposimato, and D. Roddeman (2009b), Numerical modeling of 2-D granular step collapse on erodible and nonerodible surface, *J. Geophys. Res.*, *114*, F03020, doi:10.1029/2008JF001186.

Daerr, A., and S. Douady (1999), Two types of avalanche behaviour in granular media, *Nature*, *399*, page numbers?.

Davies, T. R., M. J. McSaveney, and K. A. Hodgson (1999), A fragmentation-spreading model for long-runout rock avalanches, *Can. Geotech. J.*, *36*(6), 1096–1110.

Deboeuf, S., O. Dauchot, L. Staron, A. Mangeney, and J. P. Vilotte (2005), Memory of the unjamming transition during the cyclic tiltings of a granular pile, *Phys. Rev. E*, *72*, 051305.

Doyle, E. E., H. E. Huppert, G. Lube, H. M. Mader, and R. S. J. Sparks, (2007), Static and flowing regions in granular collapses down channels: Insights from s sedimenting shallow water model, *Phys. Fluids*, *19*, 106601.

Felix, G., and N. Thomas (2004), Relation between dry granular flow regimes and morphology of the deposits: Formation of levées in pyroclastic deposits, *Earth Planet. Sci. Lett.*, *221*, 197–231.

Fernandez-Feria, R. (2006), Dam-break flow for arbitrary slopes of the bottom, *J. Eng. Math.*, *54*, 319–331.

Fernandez-Nieto, E., F. Bouchut, D. Bresch, M. J. Castro-Diaz, and A. Mangeney (2008), A new Savage-Hutter type model for submarine avalanches and generated tsunami, *J. Comput. Phys.*, *227*(16), 7720–7754.

Fischer, R., P. Gondret, B. Perrin, and M. Rabaud, (2008), Dynamics of dry granular avalanches, *Phys. Rev. E*, *78*, 021302.

Gauer, P., and D. Issler (2003), Possible erosion mechanisms in snow avalanches, *Ann. Glaciol.*, *38*, 384–392.

Groupement De Recherche Milieux Divises (2004), On dense granular flows *Eur. Phys. J. E.*, *14*, 341–XXX.

Girolami, L., T. H. Druitt, O. Roche, and Z. Khrabrykh (2008), Propagation and hindered settling of laboratory ash flows, *J. Geophys. Res.*, *113*, B02202, doi:10.1029/2007JB005074.

Goujon, C., B. Dalloz-Dubrujeaud, and N. Thomas (2007), Bidisperse granular avalanches on inclined planes: A rich variety of behaviors, *Eur. Phys. J. E.*, *23*, 199–215.

Heinrich, P., S. Guilbourg, A. Mangeney, and R. Roche (1999), Numerical modeling of a landslide-generated tsunami following a potential explosion of the Montserrat volcano, *Phys. Chem. Earth*, *24*(2), 163–168.

Hogg, A. J. (2008), Two dimensional granular slumps down slopes, *Phys. Fluids*, *19*, 093301.

Hsu, L., E. Dietrich, and L. S. Sklar (2008), Experimental study of bedrock erosion by granular flows, *J. Geophys. Res.*, *113*, F02001, doi:10.1029/2007JF000778.

Hungr, O. (2008), Simplified models of spreading flow of dry granular material, *Can. Geotech. J.*, *45*, 1156–1168.

Hungr, O., and S. G. Evans (2004), Entrainment of debris in rock avalanches: An analysis of a long run-out mechanism, *Bull. Geol. Soc. Am.*, *116*, 1240–1252.

Hungr, O., G. C. Morgan, and R. Kellerhals (1984), Quantitative analysis of debris torrent hazards for design of remedial measures, *Can. Geotech. J.*, *21*, 663–677.

Hungr, O., S. G. Evans, M. Bovis, and J. N. Hutchinson (2001), Review of the classification of landslides of the flow type, *Environ. Eng. Geosci.*, *12*, 221–238.

Hungr, O., J. Corominas, and E. Eberhardt (2005), Estimating landslide motion mechanism, travel distance and velocity, in *Landslide Risk Management*, edited by O. Hungr et al., page numbers?, Taylor and Francis, London.

Iverson, R. M., and R. P. Denlinger (2001), Flow of variably fluidized granular masses across three-dimensional terrain: 1. Coulomb mixture theory, *J. Geophy. Res.*, *106*(B1), 537–552.

Jop, P., Y. Forterre, and O. Pouliquen, (2006), A constitutive law for dense granular flows, *Nature*, *441*(8), 727–730.

Kerswell, R. R. (2005), Dam break with Coulomb friction: A model of granular slumping?, *Phys. Fluids*, *17*, 057101.

Kuo, C. Y., Y. C. Tai, F. Bouchut, A. Mangeney, M. Pelanti, R. F. Chen, and K. J. Chang (2009), Simulation of Tsaoling Landslide, Taiwan, based on Saint Venant equations over general topography, *Eng. Geol.*, *104*(3–4), 181–189.

Lacaze, L., J. C. Phillips, and R. R. Kerswell (2008), Planar collapse of a granular column: Experiments and discrete element simulations, *Phys. Fluids*, *20*, 063302.

Lahousse, P., and P. G. Salvador (1995), The torrential flood of the Bez (French Alps, Brianconnais), July 24th, *Geodin. Acta*, *11*(4) 163–170.

Lajeunesse, E., A. Mangeney-Castelnau, and J. P. Vilotte (2004), Spreading of a granular mass on a horizontal plane, *Phys. Fluids*, *16*, 2371–2381.

Legros, F. (2002), The mobility of long-runout landslides, *Eng. Geol.*, *63*, 301–331.

Lube, G., H. E. Huppert, R. S. Sparks, and M. A. Hallworth (2004), Axisymmetric collapses of granular columns, *J. Fluid Mech.*, *508*, 175.

Lube, G., H. E. Huppert, R. S. Sparks, and A. Freundt (2007), Static and flowing regions in granular collapses down channels, *Phys. Fluids*, *19*, 043301.

Lucas, A., and A. Mangeney (2007), Mobility and topographic effects for large Valles Marineris landslides on Mars, *Geophys. Res. Lett.*, *34*, L10201, doi:10.1029/2007GL029835.

Malin, M. C., and K. S. Edgett (2001), Mars Global Surveyor Mars Orbiter Camera: Interplanetary cruise through primary mission, *J. Geophys. Res.*, *106*(E10), 23,429–23,570.

Mallogi, F., J. Lanuza, B. Andreotti, and E. Clement (2006), Erosion waves: Transverse instabilities and fingering, *Europhys. Lett.*, *75*, 825.

Mangeney, A., P. Heinrich, and R. Roche (2000), Analytical solution for testing debris avalanche numerical models, *Pure Appl. Geophys.*, *157*, 1081–1096.

Mangeney, A., L. Staron, D. Volfson, and L. Tsimring (2006), Comparison between discrete and continuum modeling of granular spreading, *WSEAS Trans. Math.*, *2*(6), 373–380.

Mangeney, A., L. S. Tsimring, D. Volfson, I. S. Aranson, and F. Bouchut (2007a), Avalanche mobility induced by the presence of an erodible bed and associated entrainment, *Geophys. Res. Lett.*, *34*, L22401, doi:10.1029/2007GL031348.

Mangeney, A., F. Bouchut, N. Thomas, J. P. Vilotte, and M. O. Bristeau (2007b), Numerical modeling of self-channeling granular flows and of their levee-channel deposits, *J. Geophys. Res.*, *112*, F02017, doi:10.1029/2006JF000469.

Mangeney-Castelnau, A., J. P. Vilotte, M. O. Bristeau, B. Perthame, F. Bouchut, C. Simeoni, and S. Yerneni (2003), Numerical modeling of avalanches based on Saint-Venant equations using a kinetic scheme, *J. Geophys. Res.*, *108*(B11), 2527, doi:10.1029/2002JB002024.

Mangeney-Castelnau, A., F. Bouchut, J. P. Vilotte, E. Lajeunesse, A. Aubertin, and M. Pirulli (2005), On the use of Saint-Venant equations to simulate the spreading of a granular mass, *J. Geophys. Res.*, *110*, B09103, doi:10.1029/2004JB003161.

Mangold, N., F. Costard, and F. Forget (2003), Debris flows over sand dunes on Mars: Evidence for liquid water, *J. Geophys. Res.*, *108*(E4), 5027, doi:10.1029/2002JE001958.

Mangold, N., A. Mangeney, V. Migeon, V. Ansan, A. Lucas, D. Baratoux, and F. Bouchut (2010), Sinuous gullies on Mars: Frequency, distribution, and implications for flow properties, *J. Geophys. Res.*, doi:10.1029/2009JE003540, in press.

McDougall, S., and O. Hungr (2004), A model for the analysis of rapid landslide runout motion across three-dimensional terrain, *Can. Geotech. J.*, *41*, 1084–1097.

Papa, M. S., S. Egashira, and T. Itoh (2004). Critical conditions of bed sediment entrainment due to debris flows, *Natl. Hazards Earth Sys. Sci.*, *4*, 469–474.

Pierson, T. C. (1980), Erosion and deposition by debris flows at Mt Thomas, North Canterbury, New Zealand, *Earth Surf. Processes*, *5*, 227–247.

Pirulli, M., and A. Mangeney (2008), Result of back-analysis of the propagation of rock avalanches as a function of the assumed rheology, *Rock Mech. Rock Eng.*, *41*(1), 59–84.

Pirulli, M., M. O. Bristeau, A. Mangeney, and C. Scavia (2007), The effect of the earth pressure coefficients on the runout of granular material, *Environ. Model. Software*, *22*, 1437–1454.

Pouliquen, O. (1999), Scaling laws in granular flows down rough inclined planes, *Phys. Fluids*, *11*(3), 542–548.

Pouliquen, O., and Y. Forterre (2002), Friction law for dense granular flows: Application to the motion of a mass down a rough inclined plane, *J. Fluid Mech.*, *453*, 133–151.

Pudasaini, S. P., and K. Hutter (2007), *Avalanche Dynamics, Dynamics of Rapid Flows of Dense Granular Avalanches*, Springer, New York.

Ritter, A. (1892), Die fortpflanzung der wasserwellen, *Z. Ver. Dtsch. Ing.*, *36*(33), 947–954.

Roche, O., M. Gilbertson, J. C. Phillips, and R. S. J. Sparks (2002), Experiments on deaerating granular flows and implications for pyroclastic flow mobility, *Geophys. Res. Lett.*, *29*(16), 1792, doi:10.1029/2002GL014819.

Roche, O., M. A. Gilbertson, J. C. Phillips, and R. S. J. Sparks (2004), Experimental study of gas-fluidized granular flows with implications

for pyroclastic flow emplacement, *J. Geophys. Res.*, *109*, B10201, doi:10.1029/2003JB002916.
Roche, O., S. Montserrat, Y. Niño, and A. Tamburrino (2008), Experimental observations of water-like behavior of initially fluidized, unsteady dense granular flows and their relevance for the propagation of pyroclastic flows, *J. Geophys. Res.*, *113*, B12203, doi:10.1029/2008JB005664.
Savage, S. B. (1979), Gravity flow of cohesionless granular materials in chutes and channels, *J. Fluid Mech.*, *92*, 53–96.
Savage, S. B., and K. Hutter (1989), The motion of a finite mass of granular material down a rough incline, *J. Fluid Mech.*, *199*, 177–215.
Savage, S. B., and R. M. Iverson (2003), Surge dynamics coupled to pore-pressure evolution in debris flows, in *Debris-Flow Hazards Mitigation: Mechanics, Prediction, and Assessment*, edited by D. Rickenmann and C. L. Chen, page numbers?, IOS Press, Fairfax, Va.
Siavoshi, S., and A. Kudrolli (2005), Failure of a granular step, *Phys. Rev. E*, *71*, 051302.
Sovilla, B., and P. Bartelt (2002), Observations and modelling of snow avalanche entrainment, *Nat. Hazards Earth Syst. Sci.*, *2*, 169–179.
Sovilla, B., P. Burlando, and P. Bartelt (2006), Field experiments and numerical modeling of mass entrainment in snow avalanches, *J. Geophys. Res.*, *111*, F03007, doi:10.1029/2005JF000391.
Sparks, R. S. J., M. C. Gardeweg, E. S. Calder, and S. J. Matthews (1997), Erosion by pyroclastic flows on Lascar Volcano, Chile, *Bull. Volcanol.*, *58*, 557–565.
Stock, J. D., and W. E. Dietrich (2006), Erosion of steepland valleys by debris flows, *Geol. Soc. Am. Bull., (9/10)*, 1125–1148.
Stock, J. D., D. R. Montgomery, D. B. Collins, W. Dietrich, and L. Sklar (2005), Field measurements of incision rates followong bedrock exposure: Implications for process controls on the long profiles of valleys cut by rivers and debris flows, *Geol. Soc. Am. Bull.*, *117*(11/12), 174–194.
Stoker, J. J. (1957), Water waves, in *The Mathematical Theory with Applications*, edited by?, page numbers?, Interscience, New York.
Suwa, H., and S. Okuda (1980), Dissection of valleys by debris flows, *Z. Geomorphol. Suppl.*, *35*, 164–182.
Tai, Y. C., and C. Y. Kuo (2008), A new model of granular flows over general topography with erosion and deposition, *Acta Mech.*, *199*, 71–96.
Takahashi, T. (1991). *Debris Flow*, *IAHR Monogr.*, 165 pp., A.A. Balkema, Rotterdam.
Wang, G., K. Sassa, and H. Fukuoka (2003), Downslope volume enlargement of a debris slide-debris flow in the 1999 Hiroshima, Japan, rainstorm, *Eng. Geol.*, *69*, 309–330.
Zanuttigh, B., and A. Lamberti (2007), Instability and surge development in debris flows, *Rev. Geophys.*, *45*, RG3006, doi:10.1029/2005RG000175.

G. Faccanoni, IMATH, Btiment U-331, Université du Sud Toulon-Var, Avenue de l'université - BP. 20132, F-83957 La Garde CEDEX, France. (gloria.faccanoni@univ-tln.fr)

O. Hungr, Department of Earth and Ocean Sciences, University of British Columbia, 6339 Stores Road, Vancouver, BC V6T 1Z4, Canada. (ohungr@eos.ubc.ca)

A. Lucas and A. Mangeney, Université Paris-Diderot 7, Institut de Physique du Globe de Paris, Equipe de Sismologie, 4 place Jussieu, F-75252 Paris CEDEX 05, France. (lucas@ipgp.jussieu.fr; mangeney@ipgp.jussieu.fr)

N. Mangold, Laboratoire de Planétologie et Géodynamique de Nantes, 2, rue de la Houssinière BP 92208, F-44322 Nantes CEDEX 3, France. (Nicolas.Mangold@univ-nantes.fr)

O. Roche, Laboratoire Magma et Volcans, 5, Rue Kessler, F-63000 Clermont Ferrand, France. (O.Roche@opgc.univ-bpclermont.fr)